iScience

CellPress
OPEN ACCESS

Article

Phenotypic and functional characterization of pharmacologically expanded Vγ9Vδ2 T cells in pigtail macaques

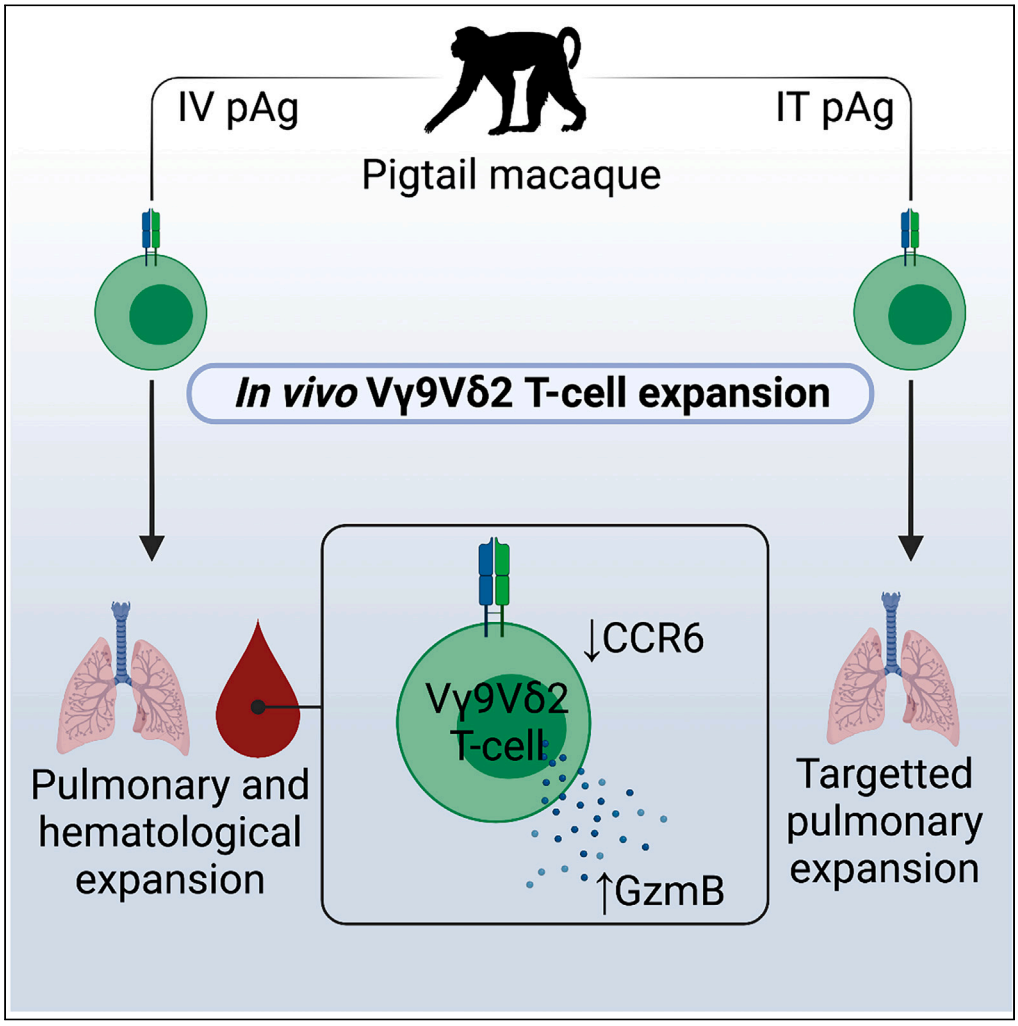

Isaac M. Barber-Axthelm, Kathleen M. Wragg, Robyn Esterbauer, ..., Anne M. Gibbon, Stephen J. Kent, Jennifer A. Juno

jennifer.juno@unimelb.edu.au

Highlights

Pigtail macaque Vγ9Vδ2 T cell subpopulations are phenotypically conserved with humans

Intratracheal phosphoantigen treatment targets expanded Vγ9Vδ2 T cells to the lungs

Pigtail macaque *in-vivo*-expanded Vγ9Vδ2 T cells in the blood lose CCR6 expression

CCR6 loss is partially dependent on rhIL-2 concentrations during *in vitro* expansion

Barber-Axthelm et al., iScience *26*, 106269
March 17, 2023
https://doi.org/10.1016/j.isci.2023.106269

iScience

CellPress
OPEN ACCESS

Article

Phenotypic and functional characterization of pharmacologically expanded Vγ9Vδ2 T cells in pigtail macaques

Isaac M. Barber-Axthelm,[1] Kathleen M. Wragg,[1] Robyn Esterbauer,[1] Thakshila H. Amarasena,[1] Valerie R.B. Barber-Axthelm,[1] Adam K. Wheatley,[1] Anne M. Gibbon,[2] Stephen J. Kent,[1,3] and Jennifer A. Juno[1,4,*]

SUMMARY

While gaining interest as treatment for cancer and infectious disease, the clinical efficacy of Vγ9Vδ2 T cell-based immunotherapeutics has to date been limited. An improved understanding of γδ T cell heterogeneity across lymphoid and non-lymphoid tissues, before and after pharmacological expansion, is required. Here, we describe the phenotype and tissue distribution of Vγ9Vδ2 T cells at steady state and following *in vivo* pharmacological expansion in pigtail macaques. Intravenous phosphoantigen administration with subcutaneous rhIL-2 drove robust expansion of Vγ9Vδ2 T cells in blood and pulmonary mucosa, while expansion was confined to the pulmonary mucosa following intratracheal antigen administration. Peripheral blood Vγ9Vδ2 T cell expansion was polyclonal, and associated with a significant loss of CCR6 expression due to IL-2-mediated receptor downregulation. Overall, we show the tissue distribution and phenotype of *in vivo* pharmacologically expanded Vγ9Vδ2 T cells can be altered based on the antigen administration route, with implications for tissue trafficking and the clinical efficacy of Vγ9Vδ2 T cell immunotherapeutics.

INTRODUCTION

Vγ9Vδ2 T cells have garnered significant interest as immunotherapeutics for both cancer and infectious disease. These cells recognize prenyl pyrophosphate antigens ("phosphoantigens") derived from microbial pathogens or host cells during times of stress. Vγ9Vδ2 T cells have a diverse functional repertoire including direct cytolysis, proinflammatory cytokine production, and antigen presentation.[1,2] Vγ9Vδ2 T cells can be readily expanded pharmacologically, with their MHC-unrestricted nature opening the possibility for "off-the-shelf" therapeutic products.[1,3–5] Multiple studies in preclinical animal models have reported promising results for both *in vivo* Vγ9Vδ2 T cell immunotherapy and adoptive transfer. However, clinical efficacy in small human trials has been limited to date.[1,6] Improving this efficacy will likely require a multifactorial approach, including refinement of treatment protocols to selectively expand clinically effective subsets of the bulk Vγ9Vδ2 T cell population, and an improved understanding of Vγ9Vδ2 T cell tissue trafficking and retention.

While Vγ9Vδ2 T cells uniformly respond to phosphoantigens, they exhibit substantial phenotypic and functional heterogeneity. Distinct human Vγ9Vδ2 T cell subsets can be defined based on expression of CCR6, CD26, CD94, and granzyme B (GzmB), which differentiate cytokine-responsive cells from cytotoxic subsets.[7–9] Whether distinct subsets can be selectively expanded *in vitro* or *in vivo* is poorly understood. Similarly, there are gaps in understanding of the tissue distribution and retention of pharmacologically expanded Vγ9Vδ2 T cells. In humans, Vγ9Vδ2 T cell expansion in the blood has been well documented following *in vivo* stimulation,[10–15] while *in-vitro*-expanded Vγ9Vδ2 T cells can be found in the blood following adoptive transfer.[16–21] In contrast, reports of Vγ9Vδ2 T cell trafficking to other tissue sites in humans are sparse. Nonhuman primate (NHP) studies have provided some evidence for Vγ9Vδ2 T cell tissue trafficking to the lungs,[22–27] gingival mucosa,[25] and rectal mucosa[25] after expansion or adoptive transfer. It is likely that successful Vγ9Vδ2 T cell-based immunotherapy will require trafficking of expanded cells to tissue sites of disease, and retention for a sufficient amount of time to exert a therapeutically beneficial effect.

[1]Department of Microbiology and Immunology, University of Melbourne, at the Peter Doherty Institute for Infection and Immunity, Melbourne, VIC 3000, Australia

[2]Monash Animal Research Platform, Monash University, Clayton, VIC 3800, Australia

[3]Melbourne Sexual Health Centre and Department of Infectious Diseases, Alfred Hospital and Central Clinical School, Monash University, Melbourne, VIC 3004, Australia

[4]Lead contact

*Correspondence: jennifer.juno@unimelb.edu.au

https://doi.org/10.1016/j.isci.2023.106269

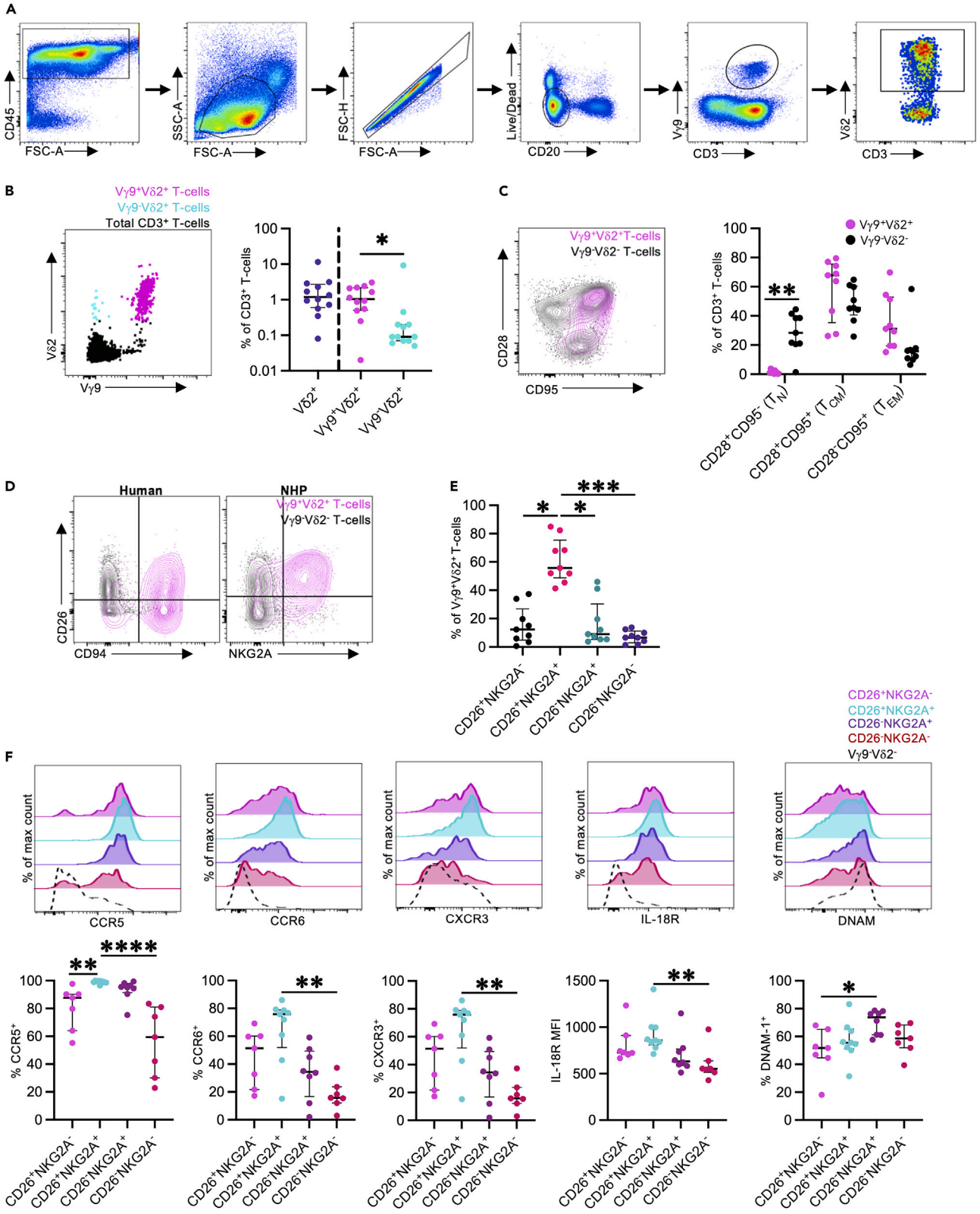
A
CD45
FSC-A
SSC-A
FSC-A
FSC-H
FSC-A
Live/Dead
CD20
Vγ9
CD3
Vδ2
CD3
B
Vγ9+Vδ2+ T-cells
Vγ9-Vδ2+ T-cells
Total CD3+ T-cells
Vδ2
Vγ9
% of CD3+ T-cells
Vδ2+
Vγ9+Vδ2+
Vγ9-Vδ2+
C
Vγ9+Vδ2+T-cells
Vγ9-Vδ2- T-cells
CD28
CD95
Vγ9+Vδ2+
Vγ9-Vδ2-
% of CD3+ T-cells
CD28+CD95- (TN)
CD28+CD95+ (TCM)
CD28-CD95+ (TEM)
D
Human
NHP
Vγ9+Vδ2+ T-cells
Vγ9-Vδ2- T-cells
CD26
CD94
NKG2A
E
% of Vγ9+Vδ2+ T-cells
CD26+NKG2A-
CD26+NKG2A+
CD26-NKG2A+
CD26-NKG2A-
F
CD26+NKG2A-
CD26+NKG2A+
CD26-NKG2A+
CD26-NKG2A-
Vγ9-Vδ2-
% of max count
CCR5
CCR6
CXCR3
IL-18R
DNAM
% CCR5+
% CCR6+
% CXCR3+
IL-18R MFI
% DNAM-1+

Figure 1. Peripheral blood Vγ9Vδ2 T cell frequencies and phenotypes

(A) Representative flow cytometry gating strategy to identify $CD3^+$ Vγ9Vδ2 T cells in cryopreserved PTM samples.

(B) Representative FACS plot and frequencies of $Vδ2^+$ T cells, $Vγ9^+Vδ2^+$ T cells, and $Vγ9^-Vδ2^+$ T cells, as a percentage of the total $CD3^+$ T cell population in peripheral blood mononuclear cells from adult male pigtail macaques (*Macaca nemestrina*). The FACS plot shows $Vγ9^+Vδ2^+$ T cells (magenta), $Vγ9^-Vδ2^+$ T cells (cyan), and total $CD3^+$ T cells (black).

(C) Representative FACS plot and frequencies of naive (T_N; $CD28^+CD95^-$), central memory (T_{CM}; $CD28^+CD95^+$), and effector memory (T_{EM}; $CD28^-CD95^+$) T cells. Plot shows $Vγ9^+Vδ2^+$ T cells (magenta) and $Vγ9^-Vδ2^-$ T cells (black).

(D) Representative FACS plots illustrating CD26 expression with CD94 (human) or NKG2A (pigtail macaque) expression, on peripheral blood Vγ9Vδ2 T cells.

(E) Frequencies of CD26/NKG2A expression on peripheral blood Vγ9Vδ2 T cells in pigtail macaques.

(F) CCR5, CCR6, CXCR3, IL-18R, and DNAM-1 expression on peripheral blood Vγ9Vδ2 T cells relative to CD26 and NKG2A co-expression.

Each point on the graphs represents an individual animal for each blood sample. Lines and error bars indicate median and interquartile range. All analysis was performed on cryopreserved PBMC samples (n = 8–12 animals from 6 to 7 independent experiments). Statistics assessed by two-tailed Wilcoxon test (B and C), Friedman test with Dunn's multiple comparisons correction (E), or Kruskal-Wallis test with Dunn's multiple comparisons correction (F). *$p < 0.05$, **$p < 0.01$, ***$p < 0.001$, ****$p < 0.0001$.

A better understanding of Vγ9Vδ2 T cell tissue trafficking, and how different expansion protocols may impact tissue trafficking, will aid in developing novel Vγ9Vδ2 T cell immunotherapies with improved clinical efficacy.

One major limitation to studying Vγ9Vδ2 T cells is the lack of relevant animal models, largely due to the lack of functional Vγ9, Vδ2, and/or relevant butyrophilin genes in most laboratory animal models.[28] NHPs are a well-suited animal model to study Vγ9Vδ2 T cells *in vivo* since they naturally develop Vγ9Vδ2 T cells and there is a growing sophistication in reagents and resources available for NHP immunology research. However, characterization of the NHP Vγ9Vδ2 T cell population remains sparse, including identifying phenotypically and functionally distinct subsets analogous to humans.

In the present study, we evaluate the phenotype and clonality of Vγ9Vδ2 T cells in pigtail macaques (*Macaca nemestrina*; PTM) at steady state and following *in vivo* pharmacological expansion. PTMs are valuable preclinical animal models for multiple infectious diseases that are relevant for Vγ9Vδ2 T cell-based therapies, including influenza,[29–31] HIV/*Mycobacteria tuberculosis* (*Mtb*) co-infection,[32] and malaria.[33] We find that phosphoantigen delivery to the airways can target *in vivo* Vγ9Vδ2 T cell expansion in the lungs, with minimal changes in peripheral blood Vγ9Vδ2 T cell frequencies. In addition, we show that phosphoantigen and recombinant human IL-2 (rhIL-2)-mediated *in vivo* expansion is associated with a loss of CCR6 expression in peripheral blood Vγ9Vδ2 T cells while maintaining Vγ9Vδ2 T cell clonal diversity.

RESULTS

Circulating PTM and human Vγ9Vδ2 T cells are phenotypically similar

While NHP Vγ9Vδ2 T cells are known to be phosphoantigen-reactive,[34] it is unclear the extent to which circulating PTM Vγ9Vδ2 T cell populations recapitulate the phenotypic and functional diversity of human cells.[7] To assess this, we analyzed Vγ9Vδ2 T cell frequencies and phenotype in cryopreserved peripheral blood mononuclear cells (PBMCs) from 8 to 12 adult PTMs (Figure 1A). Peripheral blood $Vδ2^+$ T cell frequencies were variable at 0.08%–11.5% (median: 1.19%, interquartile range [IQR]: 0.6–2.72%) of the total $CD3^+$ T cell population (Figure 1B). As expected, the majority of $Vδ2^+$ T cells co-expressed Vγ9 (median: 1.04% of $CD3^+$ T cells, IQR: 0.51%–2.17%), with a less frequent $Vγ9^-Vδ2^+$ T cell population (median: 0.09% of $CD3^+$ T cells, IQR: 0.07%–0.2%, $p = 0.0425$) (Figure 1B). The low frequency of $Vγ9^-Vδ2^+$ T cells, relative to $Vγ9^+Vδ2^+$ T cell frequencies, is consistent with human peripheral blood $Vδ2^+$ T cell patterns.[35,36] PTM peripheral blood Vγ9Vδ2 T cells primarily exhibited a central memory-like (T_{CM}; $CD28^+CD95^+$; median: 67.9%, IQR: 35.5%–75.7%) or effector memory-like phenotype (T_{EM}; $CD28^-CD95^+$; median: 31.2%, IQR: 19.5%–52.9%), with a minimal naive population (Figure 1C). These patterns are analogous to human Vγ9Vδ2 T cells.[7,37,38]

Key phenotypic and functional Vγ9Vδ2 T cell subsets can be defined based on CD26/CD94 co-expression in humans (Figure 1D),[7] and we therefore investigated if similar phenotypic subsets could be identified in PTMs. Although antibodies to detect CD94[39] in NHPs are not available, we utilized an antibody to NKG2A as a surrogate marker, which dimerizes with CD94 on human Vγ9Vδ2 T cells.[7] PTM Vγ9Vδ2 T cells were predominately $CD26^+NKG2A^+$ (median: 55.7% of Vγ9Vδ2 T cells, IQR: 48.7%–75.4%; Figure 1E). In humans, CD26/CD94 expression on peripheral blood Vγ9Vδ2 T cells is variable and donor dependent, though the $CD26^+CD94^{hi}$ subset tends to predominate in adults (comprising ~38% of the total Vγ9Vδ2

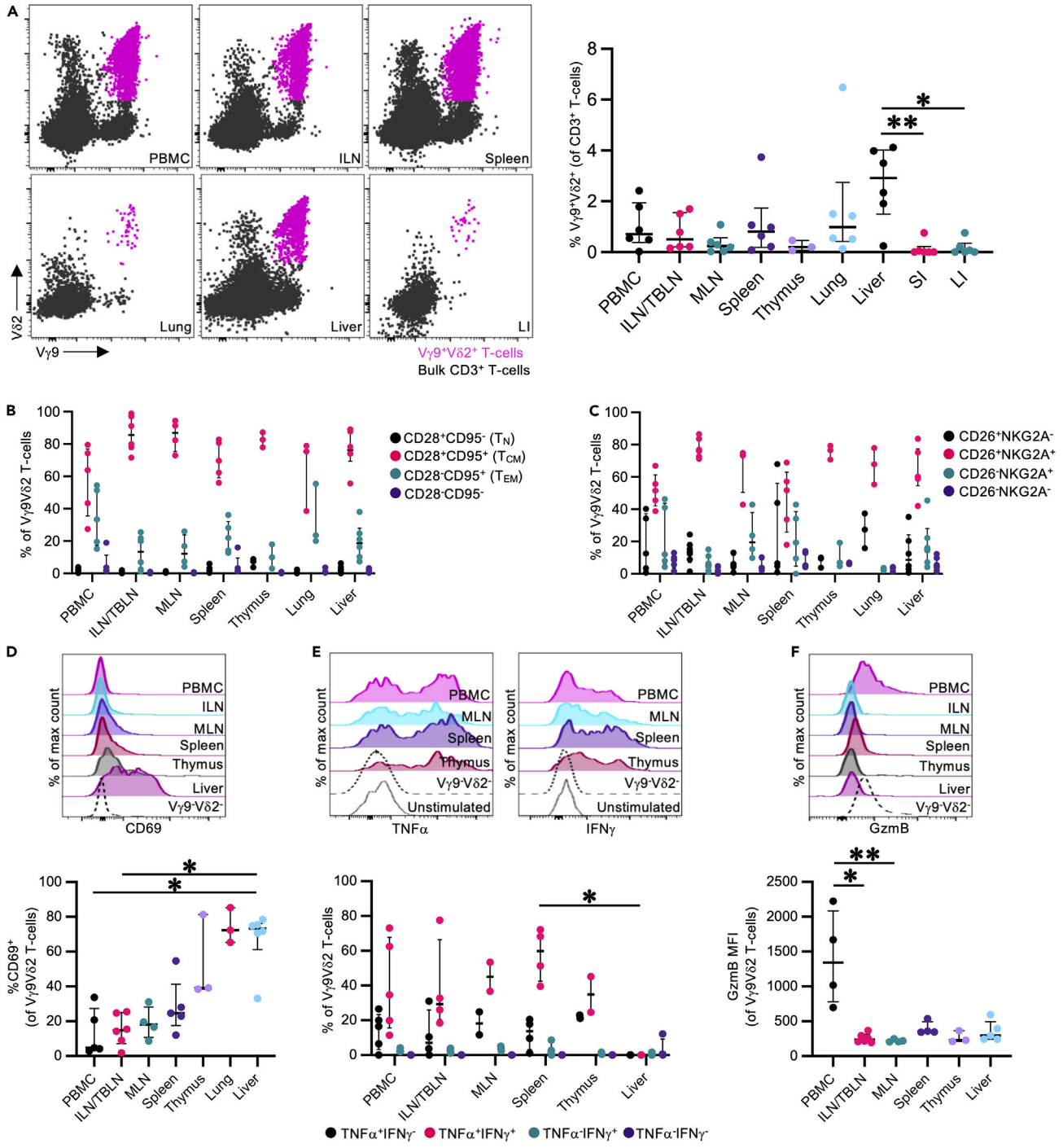

Figure 2. Frequencies and phenotypes of pigtail macaque tissue Vγ9Vδ2 T cells

Vγ9Vδ2 T cell frequencies and phenotypes were evaluated in peripheral blood mononuclear cells (PBMC), inguinal lymph nodes/tracheobronchial lymph nodes (ILN/TBLN), mesenteric lymph nodes (MLN), spleen, thymus, lung, liver, small intestine (SI), and large intestine (LI).

(A) Representative Vγ9Vδ2 T cell frequencies in paired cryopreserved PBMC and tissue samples from an adult male pigtail macaque. $CD3^+$ Vγ9Vδ2 T cells were identified based on the flow cytometry gating strategy illustrated in Figure 1A. FACS plots show Vγ9Vδ2 T cell (magenta) and bulk $CD3^+$ T cells (black).

(B) Frequencies of $CD28^+CD95^-$ (naive; T_N), $CD28^+CD95^+$ (central memory; T_{CM}), $CD28^-CD95^+$ (effector memory; T_{EM}), and $CD28^-CD95^-$ Vγ9Vδ2 T cells in peripheral blood and tissue sites.

(C) Frequencies of CD26 and NKG2A expression of peripheral blood- and tissue-derived Vγ9Vδ2 T cells.

(D) Representative histograms and frequencies of CD69 expression on peripheral blood- and tissue-derived Vγ9Vδ2 T cells.

Figure 2. *Continued*

(E) Representative histograms and frequencies of TNFα and IFNγ expression in peripheral blood- and tissue-derived Vγ9Vδ2 T cells, following a 16 h *in vitro* stimulation with HMB-PP. *In vitro* stimulation was performed as described in the method details. Cytokine production frequencies were calculated following background subtraction using paired unstimulated control samples.

(F) Representative histograms and median fluorescence intensities (MFI) of granzyme B (GzmB) expression in peripheral blood- and tissue-derived Vγ9Vδ2 T cells at steady state. Additional tissue phenotyping data presented in Figure S1.

Each point on the graphs represents an individual animal for each tissue sample. Lines and error bars indicate median and interquartile range. All analysis was performed on cryopreserved samples (n = 2–6 animals depending on tissue availability and cell recovery, from 2 to 5 independent experiments). Statistics assessed by Kruskal-Wallis test with Dunn's multiple comparisons correction (Aa dn D–F). *p < 0.05, **p < 0.01.

population).[7] Consistent with observations in human cohorts,[7] $CD26^{+}NKG2A^{+/-}$ Vγ9Vδ2 T cells expressed higher levels of the cytokine and chemokine receptors CCR5, CCR6, CXCR3, and IL-18R, relative to $CD26^{-}NKG2A^{+/-}$ Vγ9Vδ2 T cells (Figure 1F). In contrast, expression of DNAM-1, a cell adhesion molecule associated with cytotoxicity, was highest in $CD26^{-}NKG2A^{+}$ Vγ9Vδ2 T cells. In general, we find the phenotypic features of human peripheral blood Vγ9Vδ2 T cells are largely conserved across PTMs and humans.

Tissue distribution of PTM Vγ9Vδ2 T cells

While Vγ9Vδ2 T cells predominately reside in the peripheral blood, they can traffic to inflamed tissue sites.[40] However, information on Vγ9Vδ2 T cell frequencies and phenotypes across different tissue sites is limited. We evaluated the frequency and phenotype of PTM Vγ9Vδ2 T cells in PBMCs and paired tissues from 2 to 6 PTMs, including lymph nodes, spleen, thymus, lung, liver, small intestine, and large intestine. Vγ9Vδ2 T cell frequencies were highest in the liver (median: 2.9% of $CD3^{+}$ T cells, IQR: 1.5%–4.0%), lung (median: 0.99% of $CD3^{+}$ T cells, IQR: 0.4%–2.7%), and spleen (median: 0.8% of $CD3^{+}$ T cells, IQR: 0.2%–1.7%) (Figure 2A). In contrast, low Vγ9Vδ2 T cell frequencies were found in the small intestine (median: 0.0% of $CD3^{+}$ T cells, IQR: 0.0%–0.2%), large intestine (median: 0.04% of $CD3^{+}$ T cells, IQR: 0.0%–0.3%), and thymus (median: 0.2% of $CD3^{+}$ T cells, IQR: 0.06%–0.5%).

Assessment of PTM Vγ9Vδ2 phenotype across tissue sites

Across the peripheral lymphoid tissues, thymus, lung, and liver, PTM Vγ9Vδ2 T cells predominately expressed a T_{CM} surface phenotype (Figure 2B). In addition, Vγ9Vδ2 T cells in the lymph nodes, thymus, lung, and liver were predominately $CD26^{+}NKG2A^{+}$, like peripheral blood Vγ9Vδ2 T cells (Figure 2C). Similar to blood Vγ9Vδ2 T cells, Vγ9Vδ2 T cells across all the tissue sites exhibited high expression of CCR5, CCR6, CXCR3, and IL-18R; an exception being $CCR6^{+}$ Vγ9Vδ2 T cell frequencies in the lungs (median CCR6 expression 50.5% of Vγ9Vδ2 T cells, IQR: 20.5%–55.5%), which were reduced relative to the other tissue sites, but not statistically different (Figure S1A). PTM Vγ9Vδ2 T cells from all tissue sites expressed high frequencies of the transcription factor PLZF, which is associated with human Vγ9Vδ2[7,41] and other unconventional T cells[42,43] (Figure S1B). As expected, CD69 expression was lowest on peripheral blood and lymph node Vγ9Vδ2 T cells, while pulmonary and hepatic-derived Vγ9Vδ2 T cells expressed high levels of CD69, consistent with its role in identifying tissue-resident lymphocytes (Figure 2D).[44,45] Despite reports of T follicular helper (T_{FH})-like $CXCR5^{+}$ Vγ9Vδ2 T cells in blood and peripheral lymphoid tissues of humans,[46] we found minimal evidence for $CXCR5^{+}$ Vγ9Vδ2 T cells in PTMs (Figure S1C). PTM Vγ9Vδ2 T cells also exhibited low Bcl6 expression, the canonical T_{FH} transcription factor.[47] Thymic Vγ9Vδ2 T cell Bcl6 expression was relatively increased compared to the other tissue sites, which may be a necessity for thymic Vγ9Vδ2 T cell development as with invariant natural killer T cells and mucosal-associated invariant T cells (MAIT cells).[48]

Functional capacity of tissue-specific Vγ9Vδ2 T cells

Given that PTM Vγ9Vδ2 T cells express both CXCR3 (a T_H1-associated marker) and CCR6 (a T_H17-associated marker),[47] we next assessed cytokine production profiles across tissue sites via *in vitro* phosphoantigen stimulation. PTM Vγ9Vδ2 T cells showed high TNFα and IFNγ expression following (E)-1-Hydroxy-2-methyl-2-butenyl 4-pyrophosphate (HMB-PP; 20 ng/mL) stimulation (Figure 2E) with minimal IL-17A or GM-CSF expression (Figure S1D), which is consistent with previous Vγ9Vδ2 T cell studies in humans[49–52] and NHPs.[22,23,53] Across all sites, Vγ9Vδ2 T cells expressed high levels of Eomes, with variable T-bet expression (Figure S1E); these two transcription factors are associated with T_H1 conventional T cell differentiation, consistent with the observed TNFα and IFNγ expression.[47] Altogether, PTM Vγ9Vδ2 T cells express high levels of cytokine and chemokine surface receptors, as well as a T_H1 cytokine profile following phosphoantigen stimulation. This surface receptor and cytokine profile is consistent with an "innate-like effector"

transcriptional profile present in human Vγ9Vδ2 T cells.[41] Additionally, unlike conventional T_H17 cells, we see dissociation between CCR6 and IL-17A expression.

DNAM-1[54,55] and GzmB[9] are both important markers for mediating cytotoxic activity against target cells and may be relevant in the context of Vγ9Vδ2 T cell-based immunotherapies. DNAM-1 expression in PTM Vγ9Vδ2 T cells was variable across the tissue sites and between individuals (Figure S1F). Pulmonary (median: 13.7% of Vγ9Vδ2 T cells, IQR: 6.0%–18.0%) and thymic (median: 14.1% of Vγ9Vδ2 T cells, IQR: 9.3%–22.1%) Vγ9Vδ2 T cells exhibited reduced DNAM-1 expression relative to other anatomic sites, which could indicate reduced cytolytic function of steady-state Vγ9Vδ2 T cells in these tissue sites. Likewise, GzmB expression was markedly reduced in all tissue-derived Vγ9Vδ2 T cells relative to peripheral blood Vγ9Vδ2 T cells (Figure 2F).

Antigen administration route influences the tissue distribution of *in-vivo*-expanded Vγ9Vδ2 T cells

Given the steady-state presence of Vγ9Vδ2 T cells across multiple tissues, we next evaluated the impact of *in vivo* pharmacological expansion in a small (n = 7) macaque study designed to probe the phenotype and function of expanded Vγ9Vδ2 T cells across multiple sites, with an emphasis on pulmonary tissue trafficking. Adult male PTMs were treated with 1 of 4 different antigen treatment protocols (n = 1–2 per group; Figure 3A, Table 1) along with recombinant human IL-2 (rhIL-2) to stimulate *in vivo* Vγ9Vδ2 T cell expansion. The group 1 treatment protocol (Zoledronic acid monohydrate [Zol] intravenous [IV]) models commonly utilized *in vivo* Vγ9Vδ2 T cell expansion protocols in previous human clinical trials.[13,56–59] The group 3 treatment protocol (HMB-PP IV and intratracheal [IT]) was designed to give the highest probability of *in vivo* Vγ9Vδ2 T cell expansion in the airway mucosa, by utilizing a phosphoantigen that very potently activates Vγ9Vδ2 T cells administered systemically and directly in the respiratory tract.[60] Groups 2 (Zol IT) and 4 (IPP IT) were included to evaluate if antigens that are less potent at activating Vγ9Vδ2 T cells, relative to HMB-PP, can induce *in vivo* Vγ9Vδ2 T cell expansion in the pulmonary mucosa when instilled directly in the respiratory tract. Whole blood, bronchoalveolar lavage (BAL) fluid, lymph node biopsies, and rectal mucosal biopsies were collected at regular time intervals and compared to baseline samples to evaluate the change in Vγ9Vδ2 T cell phenotype and function (Figure 3A; gating strategy to identify Vγ9Vδ2 T cells: Figure 3B).

Significant Vγ9Vδ2 T cell expansion was observed at day 4 post antigen administration in the blood (range: 12.2%–28.0% of $CD3^+$ T cells across groups 1 and 3) compared to pre-expansion frequencies (range: 0.27%–1.25% of $CD3^+$ T cells across groups 1 and 3) and was primarily restricted to animals that received intravenous antigen (Figure 3C). This was preceded by a transient decrease in Vγ9Vδ2 T cell frequencies at day 2, similar to what has been observed in *in vivo* expansion studies with anti-butyrophilin 3A (BTN3A) monoclonal antibody immunotherapy.[61] This decrease may reflect redistribution from the blood to other tissue sites, or may be due to activation-induced T cell receptor (TCR) downregulation.[62] By day 8 post antigen administration, peripheral blood Vγ9Vδ2 T cell frequencies had returned to baseline levels, indicating that the pharmacological expansion in the peripheral blood was relatively transient.

In tissue sites, Vγ9Vδ2 T cell expansion was identified in the BAL fluid of all 4 groups at day 8 post antigen administration (Figure 3D). The magnitude of change in Vγ9Vδ2 T cell frequency was considerably variable across the groups, with group 3 having the largest increase in Vγ9Vδ2 T cell frequencies (range: 10.81%–14.86% of $CD3^+$ T cells at day 8 compared to 3.95%–6.81% at day 7), and group 2 having the smallest increase (range: 3.25%–7.72% of $CD3^+$ T cells at day 8; 2.23%–6.09% at day 7). In addition, pulmonary Vγ9Vδ2 T cell frequencies remained elevated in 4/7 macaques out to day 22 post antigen administration, suggesting a level tissue retention not observed in the peripheral blood. In contrast to the respiratory tract, no significant change in Vγ9Vδ2 T cell frequencies was observed in the peripheral lymph node or rectal mucosa with any of the treatment groups (Figure 3E). Vγ9Vδ2 T cell frequencies were low in all animals' pre-treatment (Lymph node: 0.08%–0.87% of $CD3^+$ T cells at day 7; Rectal mucosa: 0.04%–0.45% of $CD3^+$ T cells at day 7) and remained consistently low throughout the observation period. These results show that changes to the antigen and route of administration can alter Vγ9Vδ2 T cell tissue distribution, with the potential for lung retention. In addition, we see that robust Vγ9Vδ2 T cell expansion in the blood does not necessarily translate to distribution in tissue sites, an important consideration for Vγ9Vδ2 T cell immunotherapies.

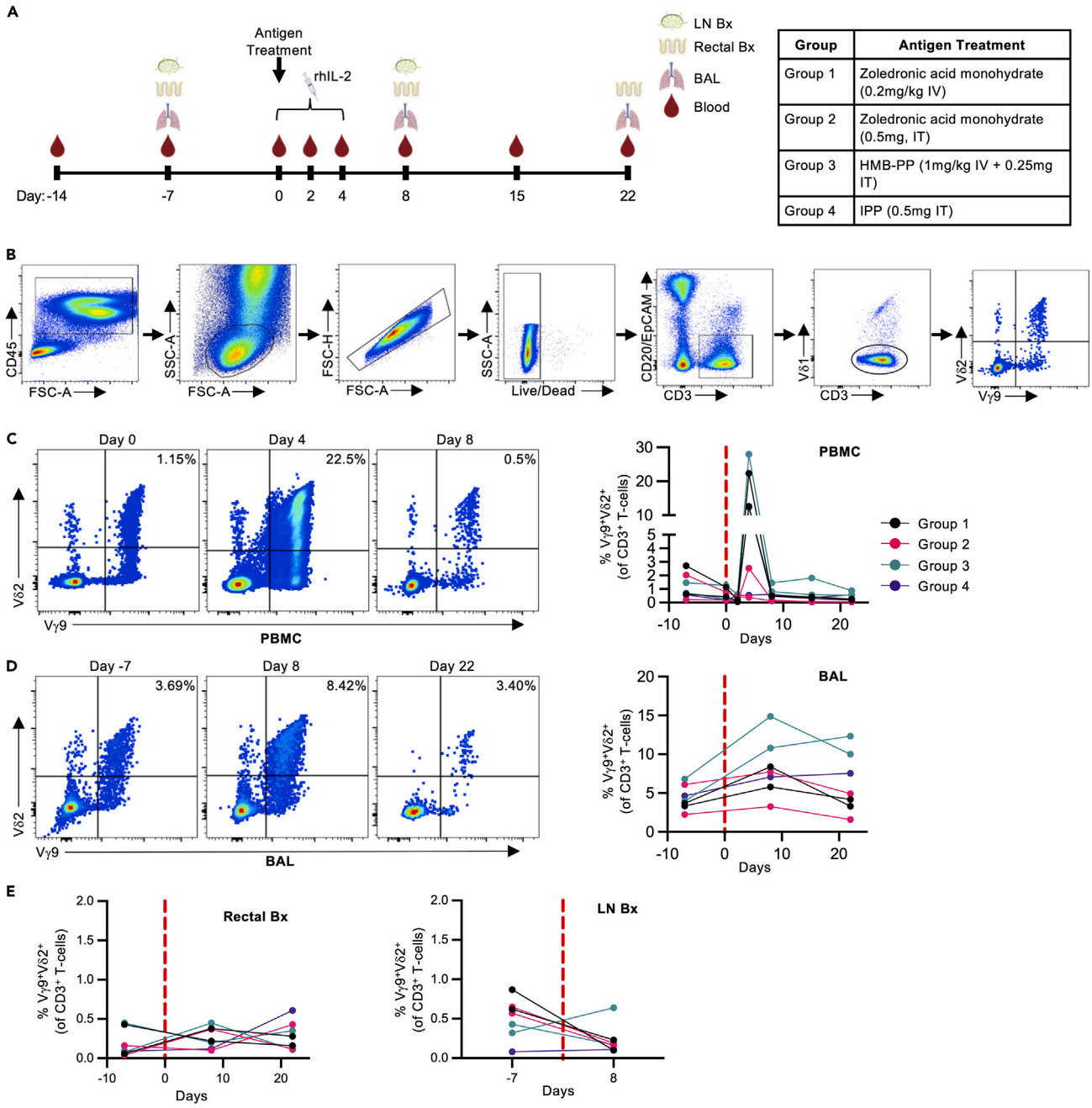

Group	Antigen Treatment
Group 1	Zoledronic acid monohydrate (0.2mg/kg IV)
Group 2	Zoledronic acid monohydrate (0.5mg, IT)
Group 3	HMB-PP (1mg/kg IV + 0.25mg IT)
Group 4	IPP (0.5mg IT)

Figure 3. *In vivo* Vγ9Vδ2 T cell expansion following antigen and rhIL-2 treatment

(A) 7 pigtail macaques were treated with 1 of 4 different antigen treatment regimens along with rhIL-2 (0.8 x10^6 IU subcutaneously q24 h for 5 days) to stimulate *in vivo* Vγ9Vδ2 T cell expansion (1–2 animals per antigen treatment group). Peripheral blood mononuclear cells (PBMC), bronchoalveolar lavage fluid (BAL), rectal mucosal biopsies (Rectal Bx), and inguinal lymph node biopsies (LN Bx) were collected at the indicated timepoints pre- and post-antigen administration. Diagram created with BioRenderer.com.

(B) $CD3^+$ Vγ9Vδ2 was identified from fresh PBMC and tissue samples using the indicated gating strategy.

(C) Representative FACS plots (Group 1) and frequencies of peripheral blood Vγ9Vδ2 T cells pre- and post-antigen and rhIL-2 treatment.

(D) Representative FACS plots (Group 1) and frequencies of Vγ9Vδ2 T cells in the BAL pre- and post-antigen and rhIL-2 administration.

(E) Vγ9Vδ2 T cell frequencies in rectal mucosa and inguinal lymph node biopsy samples pre- and post-antigen and rhIL-2 treatment.

Each point on the graphs represents an individual animal from each timepoint. Dotted red lines indicated the start of antigen and rhIL-2 treatment. Data collected from 1 experiment. IV; Intravenous, IT: Intratracheal.

Table 1. Animal and treatment group information for *in vivo* expansion trial

	Animal ID	Age (yrs)	Weight (kg)	Antigen	rhIL-2
Group 1	NM11	16	18.6	Zoledronic acid monohydrate (0.2 mg/kg IV)	$0.8x10^6$ IU SC, q24 h for 5 days
	NM89	14	21.1		
Group 2	NM88	14	13.6	Zoledronic acid monohydrate (0.5 mg, IT)	
	NM283	7	11.1		
Group 3	NM251	9	13.8	HMB-PP (1 mg/kg IV + 0.25 mg IT)	
	NM295	7	8.6		
Group 4	NM269	8	12.0	IPP (0.5 mg IT)	

Loss of CCR6 expression on *in-vivo*-expanded peripheral blood Vγ9Vδ2 T cells

We next evaluated if our *in vivo* expansion protocols caused significant changes in peripheral blood and pulmonary Vγ9Vδ2 T cell phenotype. A reduction in T_{CM}-like Vγ9Vδ2 T cells was observed across all 7 animals in the study between day 4 and day 8 ($p = 0.0334$), with a concurrent increase in T_{EM} phenotype ($p = 0.015$) (Figure 4A). This shift corresponds with contraction of the peripheral blood Vγ9Vδ2 T cell population in groups 1 and 3 animals. A transient increase in CD69 expression was observed at day 2 post antigen administration (Figure 4B), which likely reflects T cell activation following antigen and rhIL-2 administration and is consistent with findings from other Vγ9Vδ2 T cell expansion trials.[61,63] While CCR5 and CXCR3 expression remained high throughout the observation period, there was a very substantial loss of CCR6 expression within the expanded peripheral blood Vγ9Vδ2 T cells at day 4 (range: 10.4%–28.6% of Vγ9Vδ2 T cells) across groups 1 and 3 compared to pre-expansion frequencies (range: 86.3%–90.1% of Vγ9Vδ2 T cells at day 0) (Figure 4C). This effect was relatively transient, as most cells regained CCR6 expression by day 15 post antigen administration. In addition, a transient loss of CCR6 expression was also seen in the group 2 animals at day 4 (range: 13.1%–28.3% of Vγ9Vδ2 T cells; 77.3%–84.0% at day 0), despite a lack of robust expansion in the blood, suggesting the loss of CCR6 expression is not dependent on expansion. Likewise, a transient increase in GzmB expression was observed in expanded Vγ9Vδ2 T cells relative to baseline levels (Figure 4D).

In the BAL, expanded Vγ9Vδ2 T cells had a mixed T_{CM}/T_{EM} expression pattern, with considerable intra-individual variability across the groups (Figure S2A). In all animals, antigen administration was associated with a mild, progressive increase in T_{CM} Vγ9Vδ2 T cell frequencies, with a corresponding decrease in T_{EM} Vγ9Vδ2 T cells ($p = 0.0485$). Similar to the peripheral blood Vγ9Vδ2 T cells, increased CD69 expression was observed in expanded BAL Vγ9Vδ2 T cells, which was maintained throughout the observation period in 6/7 animals (Figure S2B), corresponding with the observed tissue retention within the pulmonary tree. In contrast to circulating Vγ9Vδ2 T cells, BAL-derived cells maintained relatively constant expression of CCR5, CXCR3, CCR6, and GzmB (Figures S2C and S2D). Both CCR6 (range: 38.3%–72.6% of Vγ9Vδ2 T cells at day 7) and GzmB (median fluorescence intensities [MFI]: 89.9–116 at day 7) expression were reduced in BAL Vγ9Vδ2 T cell compared to paired peripheral blood samples, with no significant or consistent change following antigen administration. In summary, we see that *in vivo* pharmacological expansion can cause significant phenotypic changes in peripheral blood Vγ9Vδ2 T cells, which may impact effector functions in a therapeutic setting. Furthermore, we see evidence of persistently increased tissue-resident Vγ9Vδ2 T cells in the airway mucosa following both IV and IT antigen administration, with no persistent changes in their phenotypic profiles from pre-expanded samples. These changes may be important when considering trafficking and functionality in different tissues.

Comparable *in vitro* expansion of $CCR6^+$ and $CCR6^-$ Vγ9Vδ2 T cells

Given that CCR6 defines a functionally and transcriptionally distinct Vγ9Vδ2 T cell population in humans,[7,9,64] we explored whether the phenotypic changes of *in-vivo*-expanded cells were due to preferential proliferation of the $CCR6^-$ subset. To address this question, we performed *in vitro* expansions with sort-purified $CCR6^+$ or $CCR6^-$ PTM Vγ9Vδ2 T cells cultured with autologous, Vδ2-depleted PBMCs (Figures 5A–5C, sort gating strategy: Figure S3). Between 2,865 and 209,300 sorted $CCR6^+$ and $CCR6^-$ Vγ9Vδ2 T cells were cultured for 13 days with Zol (15 μM), rhIL-2 ($1 x10^3$ IU/mL), and Vδ2-depleted autologous PBMCs, to evaluate differences in expansion capacity and phenotype. Paired unsorted PBMCs were also expanded under identical conditions as controls. Similar to other NHP studies,[63] there was considerable inter-individual

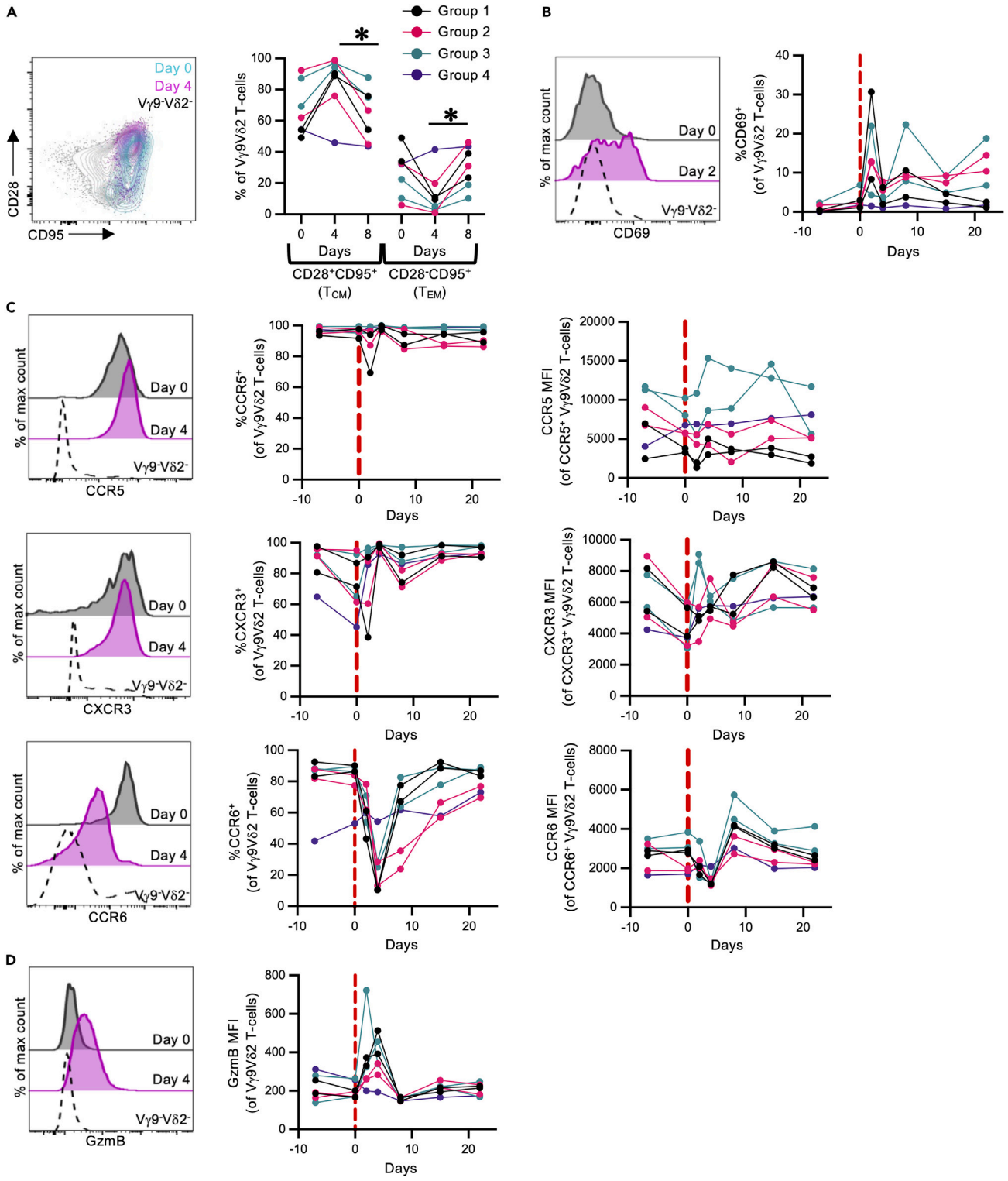

Figure 4. Phenotype of *in-vivo*-expanded Vγ9Vδ2 T cells in the blood

Phenotyping was performed on freshly isolated peripheral blood mononuclear cells (n = 7 animals; 1–2 per treatment group).

(A) Representative FACS plot and frequencies of central memory (T_{CM}; $CD28^+CD95^+$) and effector memory (T_{EM}; $CD28^-CD95^+$) Vγ9Vδ2 T cells pre- and post-antigen administration. Expanded Vγ9Vδ2 T cells (Day 4) are plotted in magenta, while pre-expanded Vγ9Vδ2 T cells (Day 0) are plotted in cyan. $Vγ9^-Vδ2^-$ T cells are plotted in black.

Figure 4. *Continued*

(B) Representative histograms and frequencies of CD69 expression on Vγ9Vδ2 T cells pre- and post-antigen administration.

(C) Representative histograms and frequencies of CCR5, CCR6, and CXCR3 on Vγ9Vδ2 T cells pre- and post-antigen administration.

(D) Representative histograms and median fluorescence intensities (MFI) of granzyme B (GzmB) expression in Vγ9Vδ2 T cells pre- and post-antigen administration.

Each point on the graphs represents an individual animal from each timepoint. Data collected from 1 experiment. Statistics assessed by Friedman test with Dunn's multiple comparisons correction across all 4 groups (A). *$p < 0.05$.

variability in Vγ9Vδ2 T cell expansion capacity. However, the fold change was comparable between CCR6$^+$ (median: 7.369, IQR: 4.1–203.1) and CCR6$^-$ Vγ9Vδ2 T cells (median: 7.942, IQR: 0.3–23.5) at the end of the expansion period, indicating that both populations expand in response to phosphoantigen and rhIL-2 stimulation (Figure 5D). Furthermore, GzmB and CCR6 expression frequencies were equivalent between the CCR6$^+$ and CCR6$^-$ cultures, as well as with autologous-expanded Vγ9Vδ2 T cells from whole PBMCs (Figure 5E). Both sorted cultures and whole PBMC cultures maintained high CXCR3 expression, like the observed *in vivo* changes (Figure 5E). Overall, these data suggest the dominant CCR6$^-$ phenotype of *in-vivo*-expanded Vγ9Vδ2 T cells likely reflects receptor downregulation rather than preferential expansion of the minor CCR6$^-$ population. Other contributing factors may include CCR6$^+$ Vγ9Vδ2 T cell trafficking into tissue compartments, as well as CCR6$^-$ Vγ9Vδ2 T cell egress from tissue compartments into the blood.

Cytokine and antigen exposure influences CCR6 and GzmB expression on PTM Vγ9Vδ2 T cells *in vitro*

We next evaluated the impact of different antigen and cytokine treatment stimuli on PTM Vγ9Vδ2 T cell phenotype to understand the mechanism of apparent CCR6 downregulation. PTM Vδ2$^+$ T cells expanded with rhIL-2 (1 x10^3 IU/mL) and Zol (15 μM), HMB-PP (20 ng/mL), or isopentenyl pyrophosphate (IPP; 4 μg/mL) had equivalent changes in CCR6 and GzmB expression patterns, as well as comparable TNFα and IFNγ responses to mitogenic stimulation (Figure S4A), indicating the antigen type does not significantly influence the phenotypic changes or cytokine production capacity of expanded PTM Vδ2 T cells. In contrast, altering rhIL-2 concentrations (0.1, 0.5, or 1 x10^3 IU/mL) caused a titratable shift in expanded Vδ2 T cell phenotypes, where rhIL-2 concentration inversely correlated with CCR6 expression frequency, and directly correlated with GzmB expression frequency (Figure 6A and 6B). Vδ2 T cell recoveries were equivalent between expansions with high, medium, and low rhIL-2 concentrations, suggesting the changes in rhIL-2 concentration did not significantly impact Vδ2 T cell proliferation of survival (Figure S4B). *In-vitro*-expanded Vδ2 T cells consistently express TNFα and IFNγ following mitogenic stimulation with minimal GM-CSF and IL-17A expression, indicating their T_H1-predominate cytokine expression profile is not affected by rhIL-2 concentrations (Figure S4C). Overall, our findings suggest that GzmB and CCR6 expression during antigen stimulation can be directly influenced by rhIL-2 concentrations.

In addition to evaluating cytokine and antigen exposure influence on expanded PTM Vγ9Vδ2 T cells, we also evaluated the phenotype of short-term Vγ9Vδ2 T cell stimulations. Cryopreserved PTM splenocytes were stimulated for 72 h with rhIL-2 or recombinant rhesus macaque IL-12 (rmIL-12) and IL-18 (rmIL-18), with or without phosphoantigen, to drive phenotypic changes in the Vγ9Vδ2 T cell population. Compared to unstimulated control samples, stimulation with rhIL-2 alone caused no significant changes in CCR6 expression (Figure 6C). However, CCR6 expression decreased in samples co-stimulated with rhIL-2 and antigen, or rmIL-12/rmIL-18 with or without antigen. Similarly, GzmB (Figure 6D) and IL-18R (Figure S5) expression was enhanced by stimulation with antigen and/or rmIL-12/rmIL-18. Overall, we find that both antigen-dependent and -independent activation of Vγ9Vδ2 T cells drives concurrent phenotypic changes, including the downregulation of CCR6 and upregulation of GzmB. Notably, rhIL-2 concentration appeared to be the primary factor influencing CCR6 downregulation, suggesting that subtle changes in Vγ9Vδ2 stimulation protocols can impact the resulting therapeutic product or *in vivo* outcome.

Peripheral blood Vγ9Vδ2 T cells maintain clonal diversity following *in vivo* expansion

While Vγ9Vδ2 T cells uniformly recognize phosphoantigens, they still undergo V(D)J recombination and generation of different clonotypes identical to conventional T cells. These different clonotypes have different functional binding avidities to target cells[65] and likely respond to different pathogenic stimuli.[66] To evaluate if our phosphoantigen/rhIL-2 *in vivo* expansion protocols selectively expanded specific clonotypes, we performed paired, single-cell TCR sequence analysis of peripheral blood Vγ9Vδ2 T cells pre-expansion (day 14) and during peak expansion (day 4) in 4 animals (Groups 1 and 3) (Table 2). Between

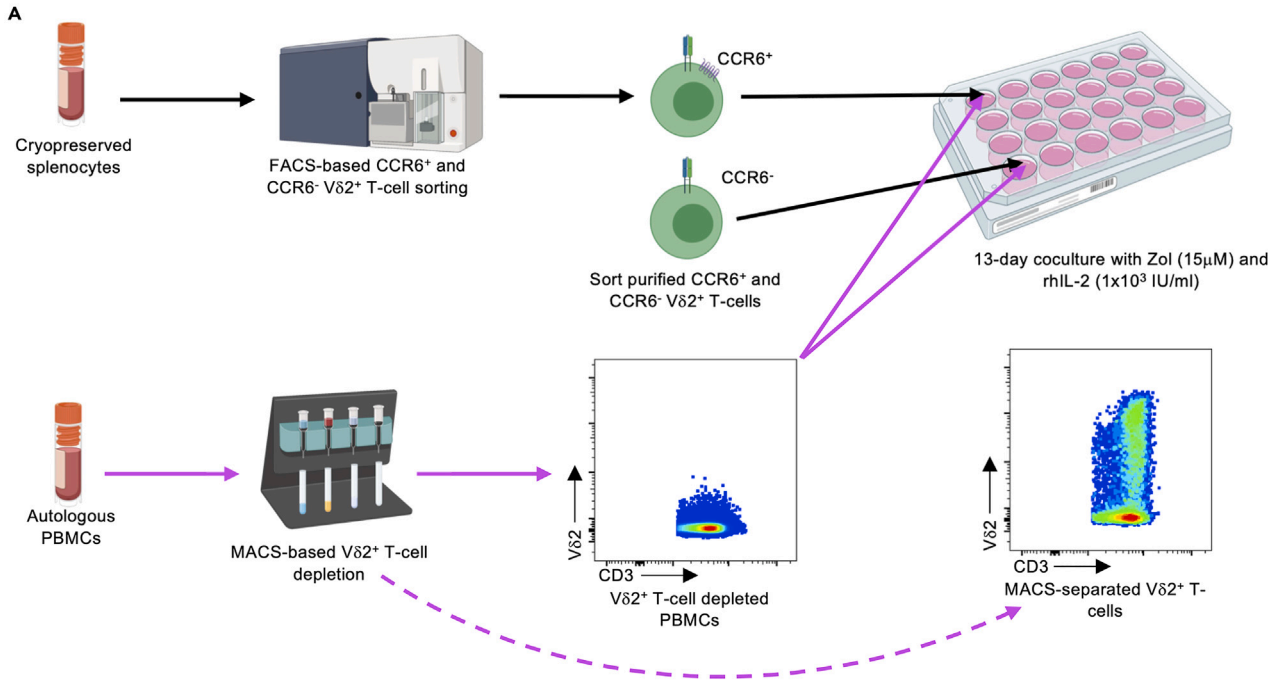
A
Cryopreserved splenocytes
FACS-based CCR6+ and CCR6- Vδ2+ T-cell sorting
CCR6+
CCR6-
Sort purified CCR6+ and CCR6- Vδ2+ T-cells
13-day coculture with Zol (15μM) and rhIL-2 (1x10³ IU/ml)
Autologous PBMCs
MACS-based Vδ2+ T-cell depletion
Vδ2
CD3
Vδ2+ T-cell depleted PBMCs
MACS-separated Vδ2+ T-cells

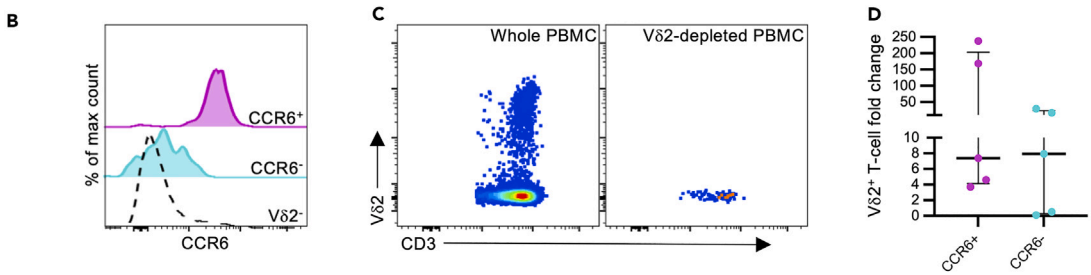
B
% of max count
CCR6+
CCR6-
Vδ2-
CCR6
C
Whole PBMC
Vδ2-depleted PBMC
Vδ2
CD3
D
Vδ2+ T-cell fold change
CCR6+
CCR6-

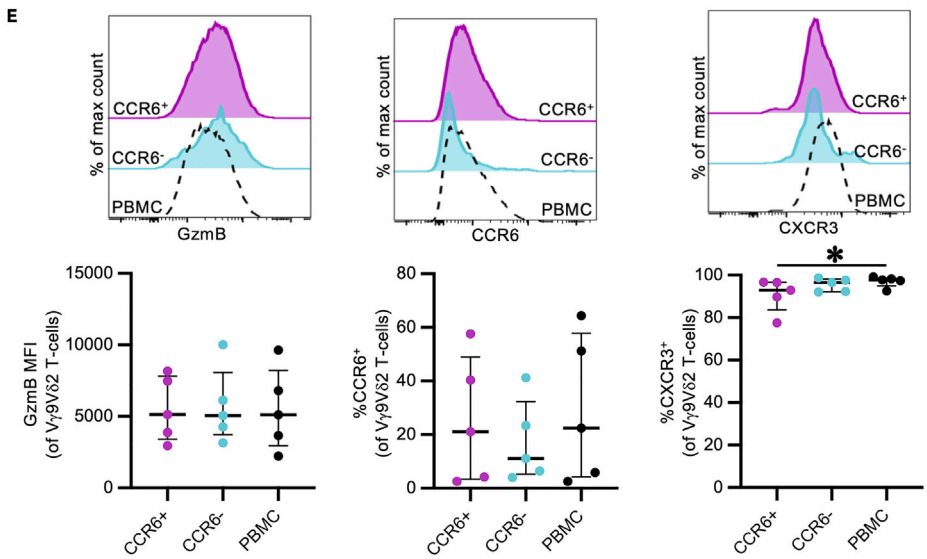
E
% of max count
CCR6+
CCR6-
PBMC
GzmB
CCR6
CXCR3
GzmB MFI (of Vγ9Vδ2 T-cells)
%CCR6+ (of Vγ9Vδ2 T-cells)
%CXCR3+ (of Vγ9Vδ2 T-cells)
CCR6+
CCR6-
PBMC

Figure 5. *In vitro* expansion of CCR6-sorted Vδ2$^+$ T cells

CCR6$^+$ and CCR6$^-$ CD3$^+$Vδ2$^+$ T cells were sort purified from cryopreserved pigtail macaque splenocytes, and expanded for 13 days in autologous, Vδ2-depleted PBMCs with Zol (15 μM) and rhIL-2 (1x10^3 IU/mL) (n = 5 animals from 3 independent experiments).

(A) Schematic of *in vitro* CCR6-sorted Vδ2$^+$ T cell expansion with Vδ2-depleted PBMCs. Diagram created with BioRenderer.com.

(B) Representative histogram of sorted CCR6$^+$ (magenta) and CCR6$^-$ (cyan) Vδ2$^+$ T cells. Vδ2$^-$ T cells are plotted in black. Sort gating strategy presented in Figure S3.

(C) FACS plots illustrating MACS-based Vδ2$^+$ T cell depletion from autologous PBMCs.

(D) Fold change in expanded CCR6-sorted Vγ9Vδ2 T cells from baseline levels, calculated as described in the method details.

(E) Granzyme B (GzmB), CCR6, and CXCR3 expression on *in-vitro*-expanded, CCR6-sorted Vγ9Vδ2 T cells or whole PBMCs.

Each point on the graphs represents an individual animal for each condition. Lines and error bars indicate median and interquartile range. Statistics assessed by two-tailed Wilcoxon test (D) or Friedman test with Dunn's multiple comparisons correction (E). *p < 0.05.

99 and 147 (median: 109.5) paired TRDV2/TRGV9 sequences were recovered across all 4 animals and both timepoints for analysis (Table S1). TCRD and TCRG CDR3 length distributions remained similar between pre-expanded and expanded Vγ9Vδ2 T cells populations (Figures 7A and 7B). J-chain usage within the TCRD and TCRG also remained constant between the pre-expanded and expanded cells, with peripheral Vγ9Vδ2 T cells predominately expressing the TRDJ1*01 and TRGJ1-2*01 alleles in all 4 PTMs (Figure S6A). Surprisingly, the PTM peripheral blood Vγ9Vδ2 T cell population was very diverse at both steady state and following expansion, with no evidence of clonal selection occurring *in vivo* (Figures 7C–7E, Table S1). Between 68 and 100 unique TCRD sequences were recovered across all 4 animals and both timepoints, of which 15.0%–35.1% were identified in pre-expanded and expanded peripheral blood samples from the same animals (Figure 7F, Table S1). As expected, the total number of unique TCRG sequences was reduced relative to the TCRD sequences, with 27.7%–50.0% of the unique TCRG sequences being shared between pre-expanded and expanded samples in individual animals. Paired TCRG/TCRD had the highest number or unique clones with the lowest frequency of intra-individual sharing across timepoint due to the presence of "pseudoclonotypes", which is well established within human Vγ9Vδ2 T cells where the germline-encoded CDR3γ9 chain pairs with multiple CDR3δ2 chains (Figure S6B, Table S1).[35] In summary, we see that the PTM peripheral blood Vγ9Vδ2 T cells are clonally diverse under steady-state condition, despite a biased V- and J-chain usage. Furthermore, the polyclonality of this population is not significantly perturbed by the substantial *in vivo* expansion driven by phosphoantigen/rhIL-2 observed. This finding is relevant to human applications as clonal selection could impact Vγ9Vδ2 T cell immunotherapeutic efficacy against certain diseases.

Since Vγ9Vδ2 T cells public clonotypes have been well established in humans[6,66] and NHPs,[67] we next looked at TCRD and TCRG sequence sharing between individual animals. Within TCRD, TCRG, and paired TCRD/TCRG sequences, the majority of unique CDR3 sequences were identified in individual animals at a single timepoint, or in a single animal pre-expansion and during peak expansion (Figures S6C–S6E). Nineteen unique TCRD CDR3 sequences were identified in more than 1 PTM, between the 2 timepoints (Figure S6C). However, a conserved TCRD CDR3 sequence was not found in all 4 PTMs. In contrast, the TCRG sequences were far more conserved between individuals, with 55 unique CDR3 sequences identified in at least 2 PTMs (Figure S6D). Among these, 2 TCRG CDR3 sequences (CALWEVQQFGRKVKLF and CALWEVRQFGRKVKLF) were identified in all 4 animals at both time points, and an additional 5 sequences (CALWEAQQFGRKVKLF, CALWEGQQFGRKVKLF, CALWESQQFGRKVKLF, CALWEVRLSGRKVKLF, and CALWEVLQFGRKVKLF) were identified in all 4 animals at 1 timepoint minimum. This robust inter-individual

Table 2. Primers from single-cell RT-PCR

	Name	Sequence
External Primers	macTCRDV2- External	CAT CTA TGG CCC TGG TTT CA
	macTCRDC- External	TGG CAG TCA AGA GAA AAT TG
	macTCRGV9- External	AGA CCT GGT GAA GTC ATA C
	macTCRGC- External	GTT GCT CTT TTC TTG CC
Internal Primers: TCRD	macTCRDV2- Internal	CAG AGA GAG ATG AAG GGT CTT AC
	macTCRDC- Internal	CAC TGG GAG AGA CGA CAA TAG
Internal Primers: TCRG	macTCRGV9- Internal	CCT GGT GAA GTC ATA CAG TTC C
	macTCRGC- Internal	AAT AGT GGG CTT GGG TGA AAT A

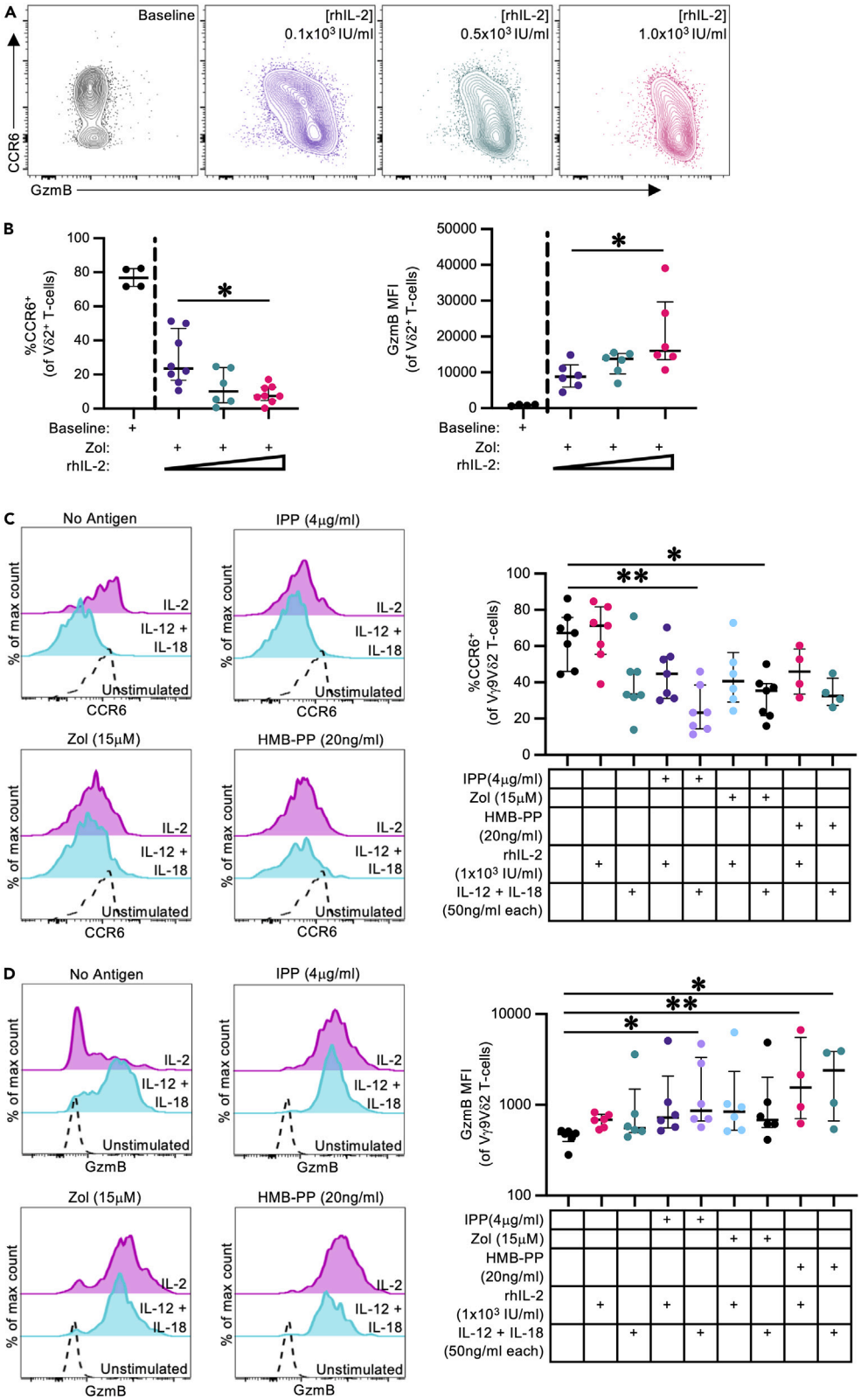
A
Baseline
[rhIL-2] 0.1x10³ IU/ml
[rhIL-2] 0.5x10³ IU/ml
[rhIL-2] 1.0x10³ IU/ml
CCR6
GzmB
B
%CCR6⁺ (of Vδ2⁺ T-cells)
GzmB MFI (of Vδ2⁺ T-cells)
Baseline:
Zol:
rhIL-2:
C
No Antigen
IPP (4μg/ml)
Zol (15μM)
HMB-PP (20ng/ml)
% of max count
IL-2
IL-12 + IL-18
Unstimulated
CCR6
%CCR6⁺ (of Vγ9Vδ2 T-cells)
IPP(4μg/ml)
Zol (15μM)
HMB-PP (20ng/ml)
rhIL-2 (1x10³ IU/ml)
IL-12 + IL-18 (50ng/ml each)
D
GzmB
GzmB MFI (of Vγ9Vδ2 T-cells)

Figure 6. Phosphoantigen and rhIL-2 driven phenotypic changes in pigtail macaque Vγ9Vδ2 T cells

Cryopreserved PBMCs (n = 8 from 4 independent experiments) were expanded *in vitro* for 13 days with Zol (15 μM) and rhIL-2 ($0.1x10^3$, $0.5x10^3$, or $1.0x10^3$ IU/mL).

(A) Representative FACS plots illustrating the shift in CCR6 and granzyme B (GzmB) expression in *in-vitro*-expanded $Vδ2^+$ T cells with increasing concentrations of rhIL-2, relative to baseline frequencies.

(B) CCR6 (%) and GzmB (MFI) expression frequencies in *in-vitro*-expanded $Vδ2^+$ T cells with increasing concentrations of rhIL-2, relative to baseline frequencies.

(C and D) Representative histograms and frequencies of CCR6 (C) and GzmB (D) expression on splenic-derived Vγ9Vδ2 T cells, following 72 h *in vitro* stimulation as described in the method details (n = 4–7 per group from 3 independent experiments). Additional data presented in Figures S4 and S5.

Each point on the graphs represents an individual animal for each condition. Lines and error bars indicate median and interquartile range. Statistic assessed by Kruskal-Wallis test with Dunn's multiple comparisons correction (B–D). *$p < 0.05$, **$p < 0.01$.

sequence conservation is likely partially due to the germline-encoded Vγ9 CDR3.[6,66] When TCRD and TCRG sequences were analyzed as pairs, the unique clonotypes were overwhelming confined to individuals, with only 3 unique sequence pairs being found in more than 1 PTM (Figure S6E). This further emphasizes the degree of clonal diversity within the bulk Vγ9Vδ2 T cell population both at steady state and following expansion, despite the presence of individual Vγ9 and Vδ2 CDR3 sharing between animals.

DISCUSSION

Fine-tuning the specificity of Vγ9Vδ2 T cell expansion protocols to produce clinically efficacious γδ T cell immunotherapies requires a detailed understanding of the heterogeneity and antigen reactivity of this unique T cell subset. NHP models provide an opportunity to probe γδ T cell immunotherapy conditions and obtain multiple tissue samples. Here, we provide a comprehensive phenotypic analysis of Vγ9Vδ2 T cells in PTMs, a relevant preclinical animal model for Vγ9Vδ2 T cell research. At steady state, we found that PTM Vγ9Vδ2 T cells are predominately $PLZF^+$, $CCR5^+$, $CCR6^+$, $CXCR3^+$, and $IL\text{-}18R^+$ across peripheral blood and tissue sites. This expression pattern is comparable with $CD26^{hi}CD94^+$ Vγ9Vδ2 T cells and MAIT cells in humans,[7] as well as MAIT cells in PTMs.[68] Analogous to humans and other NHPs, PTM Vγ9Vδ2 T cells are also biased toward a T_H1 cytokine response at steady state and following *in vitro* pharmacological expansion with phosphoantigen and rhIL-2. Following pharmacological expansion, PTM Vγ9Vδ2 T cells lose CCR6 expression both *in vivo* and *in vitro*, which is dependent on antigen and IL-2 stimulation.

PTM Vγ9Vδ2 T cell frequencies rapidly but transiently increased in the peripheral blood following IV HMB-PP or Zol, consistent with previous *in vivo* expansion trials in humans[10,13,69] and NHPs.[25,53,63] Furthermore, intravenous antigen administration resulted in Vγ9Vδ2 T cell expansion in the pulmonary mucosa, which could be targeted specifically to the pulmonary tract with IT antigen administration. Targeted Vγ9Vδ2 T cell delivery to the lungs may be beneficial therapeutically for pulmonary-based diseases like *Mtb*, against which Vγ9Vδ2 T cells have demonstrated antimicrobial activity.[22,70] Both *in-vivo*-expanded[24] and adoptively transferred[22] Vγ9Vδ2 T cells have been shown to reduce *Mtb* disease burden in NHPs, underscoring their utility as immunotherapeutics. Our results highlight how antigen delivery routes can influence the tissue distribution of expanded Vγ9Vδ2 T cells.

The rapid downregulation of CCR6 expression on expanded Vγ9Vδ2 T cells may have implications for tissue trafficking/retention of these cells during immunotherapy, as well as provide insight into the development and differentiation of $CCR6^-$ Vγ9Vδ2 T cells. CCR6 downregulation was also observed with *in-vitro*-expanded PTM Vγ9Vδ2 T cells, indicating these same tissue trafficking implications may also apply to *ex-vivo*-expanded Vγ9Vδ2 T cells for adoptive transfer. CCR6 mediates immune cell trafficking and retention in multiple anatomical and microanatomical sites, including gut-associated lymphoid tissues,[71–74] lymph node subcapsular sinuses,[75] liver,[76,77] and lung.[78,79] Pharmacological CCR6 downregulation on expanded Vγ9Vδ2 T cells may have hindered distribution to some sites in the present study, such as the rectal mucosa and lymph node. Expanded Vγ9Vδ2 T cell retention in the airway mucosa is likely due to other chemotactic receptors that were expressed throughout the expansion period, like CCR5 and CXCR3. Although Ali et al.[25] identified expanded Vγ9Vδ2 T cells in the rectal mucosa of cynomolgus macaques (*Macaca fascicularis*) following IV HMB-PP treatment, differences in HMB-PP dosages, timing between antigen administration and rectal mucosal sampling, and NHP species may explain the differences in these studies.

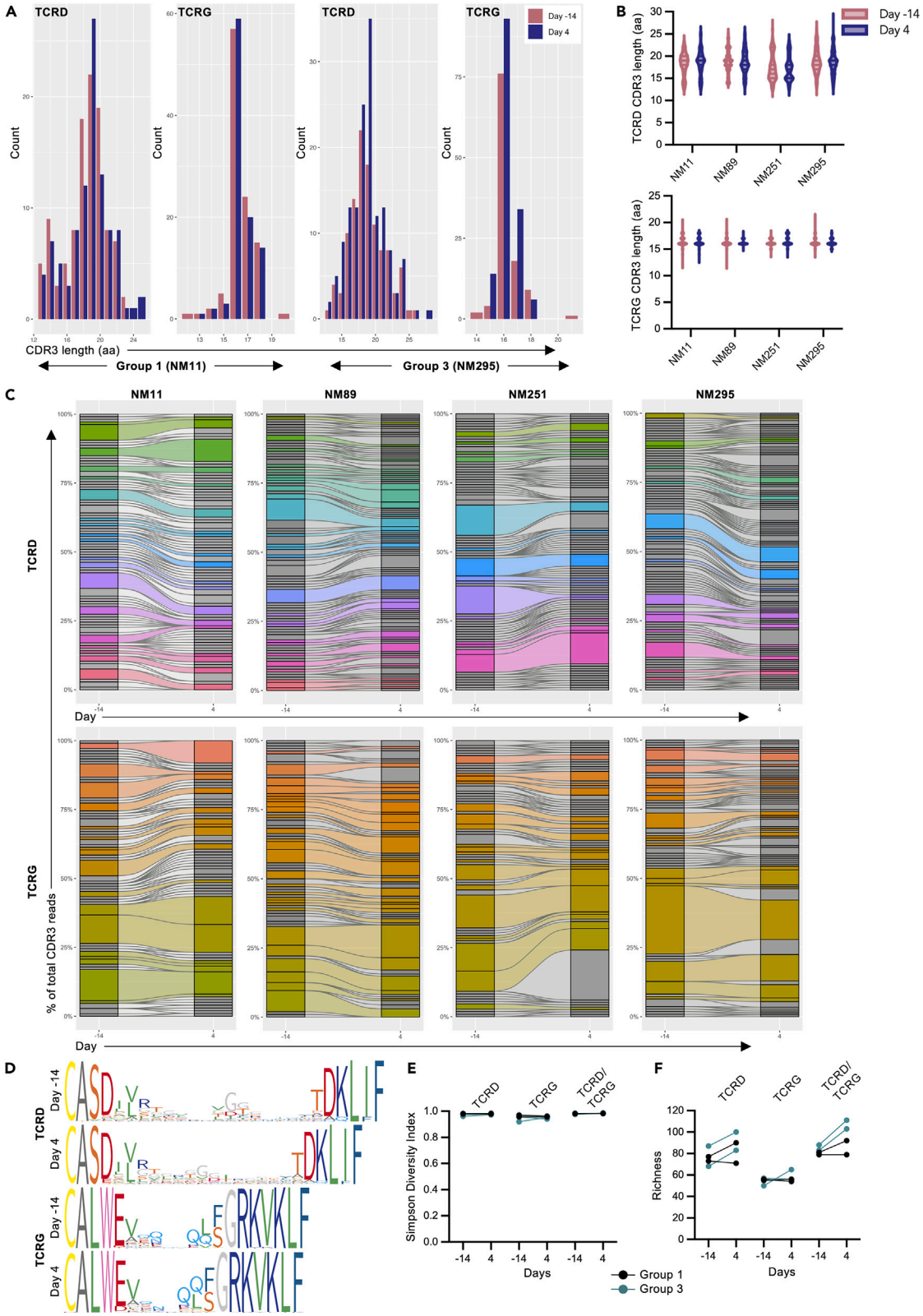
A
TCRD
TCRG
TCRD
TCRG
Day -14
Day 4
Count
CDR3 length (aa)
Group 1 (NM11)
Group 3 (NM295)
B
TCRD CDR3 length (aa)
TCRG CDR3 length (aa)
NM11
NM89
NM251
NM295
C
NM11
NM89
NM251
NM295
TCRD
TCRG
Day
% of total CDR3 reads
D
TCRD
TCRG
Day -14
Day 4
E
Simpson Diversity Index
TCRD
TCRG
TCRD/
TCRG
Days
Group 1
Group 3
F
Richness
Days

Figure 7. Clonality of *in-vivo*-expanded Vγ9Vδ2 T cells in pigtail macaques

Clonality was assessed by paired gamma and delta chain sequencing from peripheral blood Vγ9Vδ2 T cells pre-expansion (day 14) and during peak expansion (day 4) (n = 4 animals from 1 experiment).

(A) Representative TCRD and TCRG CDR3 amino acid length distributions in peripheral blood Vγ9Vδ2 T cells from a group 1 animal (NM11) and a group 3 animal (NM295).

(B) TCRD and TCRG CDR3 amino acid length distributions across all 4 PTMs pre-expansion (day 14, red) and during peak expansion (day 4, purple).

(C) TCRD and TCRG clonal diversity and clonotype sharing within each individual animal pre-expansion and during peak expansion. Gray bar segments represent individual clonotypes that were identified at 1 timepoint, while colored segments illustrate clonotypes that were shared between both timepoints.

(D) Sequence logos generated from all TCRD or TCRG CDR3 amino acid sequences from 1 animal (ClustalW alignment algorithm). Narrower bars in the logos represent gaps in the sequence. Individual amino acids are colored according to the RasMol amino color scheme.

(E) Simpson diversity index for Vγ9Vδ2 T cell TCRD, TCRG, and paired TCRD/TCRG clonotypes.

(F) Unique clonotype frequencies (richness) for Vγ9Vδ2 T cell TCRD, TCRG, and combined TCRD/TCRG chains. Individual points on the graphs represent an individual animal at each timepoint. p values for diversity and richness changes are presented in Table S1, and additional sequencing data are presented in Figure S6.

The impact of IL-2 concentration on CCR6 downregulation during *in vitro* γδ T cell expansion highlights the underappreciated impact of cytokine co-stimulation on Vγ9Vδ2 T cell phenotype. Several studies have demonstrated that human neonatal Vγ9Vδ2 T cell populations are dominated by $CCR6^{+}CD26^{+}$ cells,[7,8] despite the fact that this population typically forms a minority of the Vγ9Vδ2 T cell repertoire in adults. Whether recurrent *in vivo* activation and exposure to cytokines such as IL-2 drives differentiation away from a $CCR6^{+}$ phenotype is currently unknown, but should be explored in future studies.

Similar to human Vγ9Vδ2 T cells, we found that CD26 and NKG2A co-expression was associated with increased cytokine and chemokine receptor expression. However, PTM Vγ9Vδ2 T cells were strongly biased toward the $CD26^{+}NKG2A^{+}$ Vγ9Vδ2 T cells in blood and tissue sites, in contrast to humans where CD26 and CD94 expression on peripheral blood Vγ9Vδ2 T cells is more heterogeneous and donor dependent.[7] CD26 expression delineates a distinct, IL-23-responsive Vγ9Vδ2 T cell subset in humans, which are phenotypically and transcriptionally similar to MAIT cells.[7] In addition, CD26 binding to adenosine deaminase enhances TCR-independent Vγ9Vδ2 T cell activation.[7] Altogether, these findings indicate that PTM Vγ9Vδ2 T cells exhibit key characteristics of human Vγ9Vδ2 T cell subpopulations, but do not fully recapitulate the Vγ9Vδ2 T cell subpopulation diversity seen in humans. However, PTMs maintain the same predominate Vγ9Vδ2 T cell subpopulation as most adult humans ($CD26^{+}CD94^{hi}$), highlighting their value as models to study Vγ9Vδ2 T cell immunotherapies. Within PTMs, biased $CD26^{+}NKG2A^{+}$ Vγ9Vδ2 T cell frequencies may reflect species-specific differences or be a result of husbandry practices. While phosphoantigen-reactive Vγ9Vδ2 T cells have been identified in multiple NHP species,[53,63,80,81] data on Vγ9Vδ2 T cell subsets across different NHP species are lacking.

Peripheral blood Vγ9Vδ2 T cells were polyclonal following expansion with intravenous HMB-PP or Zol, consistent with previous studies looking at the clonality of phosphoantigen- and aminobisphosphonate-expanded human Vγ9Vδ2 T cells *in vitro*.[82,83] While Vγ9Vδ2 T cells uniformly recognize phosphoantigens,[66] Vγ9Vδ2 T cell clonotypes may be important in determining responsiveness to certain diseases. Multiple studies have reported oligoclonal Vγ9Vδ2 T cell selection in response to both infectious and non-infectious diseases.[66,84,85] BCG-mediated *in vitro* Vγ9Vδ2 T cell expansion selects for a subset of the human peripheral Vγ9Vδ2 T cell repertoire compared to IPP.[82] The impact of Vγ9Vδ2 T cell clonality on immunotherapeutic efficacy requires further investigation. However, our results indicate that *in vivo* pharmacological expansion with phosphoantigens or aminobisphosphonates does not selectively expand specific subsets of the Vγ9Vδ2 T cell clonal population.

In summary, we provide an extensive characterization of Vγ9Vδ2 T cells in NHPs and find both that *in vivo* Vγ9Vδ2 T cell expansion can be modulated by the route of antigen administration and that pharmacological expansion protocols can impact Vγ9Vδ2 T cell phenotypes beyond cytokine and cytolytic marker expression. This improved understanding of the phenotype, clonality, and tissue distribution of pharmacologically expanded Vγ9Vδ2 T cells in macaques provides an important step toward designing studies to most effectively target Vγ9Vδ2 T cells, to improve disease outcomes. Further studies are needed to evaluate how different antigens and dosages impact Vγ9Vδ2 T cell frequencies, phenotype, and function, across different antigen administration routes. Incorporating anti-BTN3A monoclonal antibodies[61] or nanoparticle-based antigen delivery[86,87] may help further refine Vγ9Vδ2 T cell expansion in selected tissue sites due to differences in biodistribution, tissue retention, and BTN3A receptor usage. Improved

protocols will likely need to be paired with optimized cytokine costimulatory treatments that selectively expand the most therapeutically effective Vγ9Vδ2 T cell subset and permits trafficking to the tissue(s) of interest. This deep characterization of Vγ9Vδ2 T cells in NHP provides a rational basis for designing and testing improved Vγ9Vδ2 T cell immunotherapies.

Limitations of the study

The principal limitation of our *in vivo* Vγ9Vδ2 T cell expansion trial is the small sample sizes per group. While we were able to observe trends in Vγ9Vδ2 T cell frequencies and phenotypes over the observation period, larger studies will be required to more conclusively optimize antigen delivery, particularly given the inter-animal variability in Vγ9Vδ2 T cell expansion.[63] We were unable to confirm if the transient CCR6 and GzmB phenotypic changes observed in peripheral blood Vγ9Vδ2 T cells during peak expansion (day 4) also occurred in the assessed tissue sites, due to limitations in the number and frequency of tissue samples that could be collected. All NHPs in the trial were adult males, with variability in age and bodyweight between the groups, which may have influenced our results. It is unknown how age, sex, and size impact tissue trafficking and phenotype of *in-vivo*-expanded $V\delta2^{+}V\gamma9^{+}$ T cells, but these biological variables may have an effect. Determining the clinical impact of *in vivo* γδ T cell expansion will require additional studies to evaluate cytotoxic effector functions with different pharmacological expansion protocols, and incorporating infectious challenge with relevant pathogens, such as *Mtb*.

Similar to our *in vivo* expansion trial, our *ex vivo* Vγ9Vδ2 T cell phenotyping is limited by tissue availability and Vγ9Vδ2 T cell recovery from cryopreserved samples. In-depth characterization of tissue-specific Vγ9Vδ2 T cell populations could be augmented by future studies using freshly collected samples.

STAR★METHODS

Detailed methods are provided in the online version of this paper and include the following:

- KEY RESOURCES TABLE
- RESOURCE AVAILABILITY
  - Lead contact
  - Materials availability
  - Data and code availability
- EXPERIMENTAL MODEL AND SUBJECT DETAILS
  - Non-human primate studies and samples
  - Human ethics statement
- METHOD DETAILS
  - Sample collection and processing
  - *In vitro* Vγ9Vδ2 T-cell expansion and stimulation
  - Single-cell TCR sequencing
  - PCR primer design
  - Antibodies and flow cytometry
- QUANTIFICATION AND STATISTICAL ANALYSIS

SUPPLEMENTAL INFORMATION

Supplemental information can be found online at https://doi.org/10.1016/j.isci.2023.106269.

ACKNOWLEDGMENTS

The authors would like to acknowledge and thank the Melbourne Cytometry Platform for provision of flow cytometry services, and Vanta Jameson and Magdaline Sakkas from the Melbourne Brain Center Flow Cytometry Facility for provision of sorting services. All nonhuman primate studies were conducted at the Monash Animal Research Platform Gippsland Field Station. We acknowledge and thank Irwin Ryan, Graham Shillito, and staff for provision of animal care and sample collection support throughout the animal trials. The study was funded by the NHMRC through Program (1149990) and Investigator grants (A.K.W., GNT1173433; J.A.J., GNT2009308). I.M.B.A. is supported by a Melbourne Research Scholarship through the University of Melbourne.

AUTHOR CONTRIBUTIONS

Conceptualization: I.M.B.A., S.J.K., and J.A.J.; Methodology: I.M.B.A., K.M.W., R.E., T.H.A., and A.K.W.; Software: I.M.B.A. and V.R.B.B.A.; Investigation: I.M.B.A. and K.M.W.; Resources: A.M.G.; Writing – Original Draft: I.M.B.A., S.J.K., and J.A.J.; Writing – Review & Editing: All authors; Visualization: I.M.B.A., S.J.K., and J.A.J.; Funding Acquisition: S.J.K. and J.A.J.; Supervision: S.J.K. and J.A.J.

DECLARATION OF INTERESTS

The authors declare no competing interests.

INCLUSION AND DIVERSITY

We support inclusive, diverse, and equitable conduct of research.

Received: October 25, 2022
Revised: December 22, 2022
Accepted: February 19, 2023
Published: February 25, 2023

REFERENCES

1. Hoeres, T., Smetak, M., Pretscher, D., and Wilhelm, M. (2018). Improving the efficiency of Vγ9Vδ2 T-cell immunotherapy in cancer. Front. Immunol. *9*, 800. https://doi.org/10.3389/fimmu.2018.00800.

2. Lawand, M., Déchanet-Merville, J., and Dieu-Nosjean, M.-C. (2017). Key features of gamma-delta T-cell subsets in human diseases and their immunotherapeutic implications. Front. Immunol. *8*, 761. https://doi.org/10.3389/fimmu.2017.00761.

3. Xu, Y., Xiang, Z., Alnaggar, M., Kouakanou, L., Li, J., He, J., Yang, J., Hu, Y., Chen, Y., Lin, L., et al. (2021). Allogeneic Vγ9Vδ2 T-cell immunotherapy exhibits promising clinical safety and prolongs the survival of patients with late-stage lung or liver cancer. Cell. Mol. Immunol. *18*, 427–439. https://doi.org/10.1038/s41423-020-0515-7.

4. Perez, C., Gruber, I., and Arber, C. (2020). Off-the-Shelf Allogeneic T cell therapies for cancer: Opportunities and challenges using naturally occurring "universal" donor T cells. Front. Immunol. *11*, 583716. https://doi.org/10.3389/fimmu.2020.583716.

5. Kondo, M., Izumi, T., Fujieda, N., Kondo, A., Morishita, T., Matsushita, H., and Kakimi, K. (2011). Expansion of human peripheral blood γδ T cells using zoledronate. J. Vis. Exp.3182 https://doi.org/10.3791/3182.

6. Sebestyen, Z., Prinz, I., Déchanet-Merville, J., Silva-Santos, B., and Kuball, J. (2020). Translating gammadelta (γδ) T cells and their receptors into cancer cell therapies. Nat. Rev. Drug Discov. *19*, 169–184. https://doi.org/10.1038/s41573-019-0038-z.

7. Wragg, K.M., Tan, H.-X., Kristensen, A.B., Nguyen-Robertson, C.V., Kelleher, A.D., Parsons, M.S., Wheatley, A.K., Berzins, S.P., Pellicci, D.G., Kent, S.J., and Juno, J.A. (2020). High CD26 and low CD94 expression identifies an IL-23 responsive Vδ2+ T cell subset with a MAIT cell-like transcriptional profile. Cell Rep. *31*, 107773. https://doi.org/10.1016/j.celrep.2020.107773.

8. Tan, L., Fichtner, A.S., Bruni, E., Odak, I., Sandrock, I., Bubke, A., Borchers, A., Schultze-Florey, C., Koenecke, C., Förster, R., et al. (2021). A fetal wave of human type 3 effector γδ cells with restricted TCR diversity persists into adulthood. Sci. Immunol. *6*, eabf0125. https://doi.org/10.1126/sciimmunol.abf0125.

9. Ryan, P.L., Sumaria, N., Holland, C.J., Bradford, C.M., Izotova, N., Grandjean, C.L., Jawad, A.S., Bergmeier, L.A., and Pennington, D.J. (2016). Heterogeneous yet stable Vδ2(+) T-cell profiles define distinct cytotoxic effector potentials in healthy human individuals. Proc. Natl. Acad. Sci. USA *113*, 14378–14383. https://doi.org/10.1073/pnas.1611098113.

10. Wilhelm, M., Kunzmann, V., Eckstein, S., Reimer, P., Weissinger, F., Ruediger, T., and Tony, H.-P. (2003). γδ T cells for immune therapy of patients with lymphoid malignancies. Blood *102*, 200–206. https://doi.org/10.1182/blood-2002-12-3665.

11. Kunzmann, V., Bauer, E., and Wilhelm, M. (1999). γ/δ T-cell stimulation by Pamidronate. N. Engl. J. Med. *340*, 737–738. https://doi.org/10.1056/nejm199903043400914.

12. Poquet, Y., Kroca, M., Halary, F., Stenmark, S., Peyrat, M.-A., Bonneville, M., Fournié, J.J., and Sjöstedt, A. (1998). Expansion of Vγ9Vδ2 T cells is Triggered by Francisella tularensis -derived phosphoantigens in Tularemia but not after Tularemia vaccination. Infect. Immun. *66*, 2107–2114. https://doi.org/10.1128/iai.66.5.2107-2114.1998.

13. Poccia, F., Gioia, C., Martini, F., Sacchi, A., Piacentini, P., Tempestilli, M., Agrati, C., Amendola, A., Abdeddaim, A., Vlassi, C., et al. (2009). Zoledronic acid and interleukin-2 treatment improves immunocompetence in HIV-infected persons by activating Vγ9Vδ2 T cells. Aids *23*, 555–565. https://doi.org/10.1097/qad.0b013e3283244619.

14. Bertaina, A., Zorzoli, A., Petretto, A., Barbarito, G., Inglese, E., Merli, P., Lavarello, C., Brescia, L.P., De Angelis, B., Tripodi, G., et al. (2017). Zoledronic acid boosts γδ T-cell activity in children receiving αβ + T and CD19 + cell-depleted grafts from an HLA-haplo-identical donor. OncoImmunology *6*, e1216291. https://doi.org/10.1080/2162402x.2016.1216291.

15. Dieli, F., Gebbia, N., Poccia, F., Caccamo, N., Montesano, C., Fulfaro, F., Arcara, C., Valerio, M.R., Meraviglia, S., Di Sano, C., et al. (2003). Induction of γδ T-lymphocyte effector functions by bisphosphonate zoledronic acid in cancer patients in vivo. Blood *102*, 2310–2311. https://doi.org/10.1182/blood-2003-05-1655.

16. Wilhelm, M., Smetak, M., Schaefer-Eckart, K., Kimmel, B., Birkmann, J., Einsele, H., and Kunzmann, V. (2014). Successful adoptive transfer and in vivo expansion of haploidentical γδ T cells. J. Transl. Med. *12*, 45. https://doi.org/10.1186/1479-5876-12-45.

17. Bennouna, J., Bompas, E., Neidhardt, E.M., Rolland, F., Philip, I., Galéa, C., Salot, S., Saiagh, S., Audrain, M., Rimbert, M., et al. (2008). Phase-I study of Innacell γδ, an autologous cell-therapy product highly enriched in γ9δ2 T lymphocytes, in combination with IL-2, in patients with metastatic renal cell carcinoma. Cancer Immunol. Immunother. *57*, 1599–1609. https://doi.org/10.1007/s00262-008-0491-8.

18. Sakamoto, M., Nakajima, J., Murakawa, T., Fukami, T., Yoshida, Y., Murayama, T., Takamoto, S., Matsushita, H., and Kakimi, K. (2011). Adoptive immunotherapy for advanced non-small cell lung cancer using zoledronate-expanded γδ T cells. J. Immunother. *34*, 202–211. https://doi.org/10.1097/cji.0b013e318207ecfb.

19. Noguchi, A., Kaneko, T., Kamigaki, T., Fujimoto, K., Ozawa, M., Saito, M., Ariyoshi, N., and Goto, S. (2011). Zoledronate-activated Vγ9γδ T cell-based

immunotherapy is feasible and restores the impairment of γδ T cells in patients with solid tumors. Cytotherapy *13*, 92–97. https://doi.org/10.3109/14653249.2010.515581.

20. Abe, Y., Muto, M., Nieda, M., Nakagawa, Y., Nicol, A., Kaneko, T., Goto, S., Yokokawa, K., and Suzuki, K. (2009). Clinical and immunological evaluation of zoledronate-activated Vγ9γδ T-cell-based immunotherapy for patients with multiple myeloma. Exp. Hematol. *37*, 956–968. https://doi.org/10.1016/j.exphem.2009.04.008.

21. Nakajima, J., Murakawa, T., Fukami, T., Goto, S., Kaneko, T., Yoshida, Y., Takamoto, S., and Kakimi, K. (2010). A phase I study of adoptive immunotherapy for recurrent non-small-cell lung cancer patients with autologous γδ T cells. Eur. J. Cardio. Thorac. Surg. *37*, 1191–1197. https://doi.org/10.1016/j.ejcts.2009.11.051.

22. Qaqish, A., Huang, D., Chen, C.Y., Zhang, Z., Wang, R., Li, S., Yang, E., Lu, Y., Larsen, M.H., Jacobs, W.R., et al. (2017). Adoptive transfer of phosphoantigen-specific γδ T cell subset Attenuates Mycobacterium tuberculosis infection in nonhuman primates. J. Immunol. *198*, 4753–4763. https://doi.org/10.4049/jimmunol.1602019.

23. Shen, L., Frencher, J., Huang, D., Wang, W., Yang, E., Chen, C.Y., Zhang, Z., Wang, R., Qaqish, A., Larsen, M.H., et al. (2019). Immunization of Vγ2Vδ2 T cells programs sustained effector memory responses that control tuberculosis in nonhuman primates. Proc. Natl. Acad. Sci. USA *116*, 6371–6378. https://doi.org/10.1073/pnas.1811380116.

24. Chen, C.Y., Yao, S., Huang, D., Wei, H., Sicard, H., Zeng, G., Jomaa, H., Larsen, M.H., Jacobs, W.R., Wang, R., et al. (2013). Phosphoantigen/IL2 expansion and differentiation of Vγ2Vδ2 T cells increase Resistance to tuberculosis in nonhuman primates. PLoS Pathog. *9*, e1003501. https://doi.org/10.1371/journal.ppat.1003501.

25. Ali, Z., Shao, L., Halliday, L., Reichenberg, A., Hintz, M., Jomaa, H., and Chen, Z.W. (2007). Prolonged (E)-4-Hydroxy-3-Methyl-But-2-Enyl pyrophosphate-driven antimicrobial and cytotoxic responses of pulmonary and systemic Vγ2Vδ2 T cells in macaques. J. Immunol. *179*, 8287–8296. https://doi.org/10.4049/jimmunol.179.12.8287.

26. Huang, D., Chen, C.Y., Ali, Z., Shao, L., Shen, L., Lockman, H.A., Barnewall, R.E., Sabourin, C., Eestep, J., Reichenberg, A., et al. (2009). Antigen-specific Vgamma2Vdelta2 T effector cells confer homeostatic protection against pneumonic plaque lesions. Proc. Natl. Acad. Sci. USA *106*, 7553–7558. https://doi.org/10.1073/pnas.0811250106.

27. Ryan-Payseur, B., Frencher, J., Shen, L., Chen, C.Y., Huang, D., and Chen, Z.W. (2012). Multieffector-functional immune responses of HMBPP-specific Vγ2Vδ2 T cells in nonhuman primates Inoculated with Listeria monocytogenes ΔactA prfA. J. Immunol. *189*, 1285–1293. https://doi.org/10.4049/jimmunol.1200641.

28. Karunakaran, M.M., Göbel, T.W., Starick, L., Walter, L., and Herrmann, T. (2014). Vγ9 and Vδ2 T cell antigen receptor genes and butyrophilin 3 (BTN3) emerged with placental mammals and are concomitantly preserved in selected species like alpaca (Vicugna pacos). Immunogenetics *66*, 243–254. https://doi.org/10.1007/s00251-014-0763-8.

29. Jegaskanda, S., Amarasena, T.H., Laurie, K.L., Tan, H.-X., Butler, J., Parsons, M.S., Alcantara, S., Petravic, J., Davenport, M.P., Hurt, A.C., et al. (2013). Standard Trivalent influenza virus Protein vaccination does not Prime antibody-dependent Cellular cytotoxicity in macaques. J. Virol. *87*, 13706–13718. https://doi.org/10.1128/jvi.01666-13.

30. Baskin, C.R., García-Sastre, A., Tumpey, T.M., Bielefeldt-Ohmann, H., Carter, V.S., Nistal-Villán, E., and Katze, M.G. (2004). Integration of clinical data, Pathology, and cDNA Microarrays in influenza virus-infected pigtailed macaques (Macaca nemestrina). J. Virol. *78*, 10420–10432. https://doi.org/10.1128/jvi.78.19.10420-10432.2004.

31. Baas, T., Baskin, C.R., Diamond, D.L., García-Sastre, A., Bielefeldt-Ohmann, H., Tumpey, T.M., Thomas, M.J., Carter, V.S., Teal, T.H., Van Hoeven, N., et al. (2006). Integrated molecular Signature of disease: analysis of influenza virus-infected macaques through functional Genomics and Proteomics. J. Virol. *80*, 10813–10828. https://doi.org/10.1128/jvi.00851-06.

32. Shen, Y., Shen, L., Sehgal, P., Huang, D., Qiu, L., Du, G., Letvin, N.L., and Chen, Z.W. (2004). Clinical Latency and Reactivation of AIDS-Related Mycobacterial infections. J. Virol. *78*, 14023–14032. https://doi.org/10.1128/jvi.78.24.14023-14032.2004.

33. Chakravarty, S., Shears, M.J., James, E.R., Rai, U., KC, N., Conteh, S., Lambert, L.E., Duffy, P.E., Murphy, S.C., and Hoffman, S.L. (2022). Efficient infection of non-human primates with purified, cryopreserved Plasmodium knowlesi sporozoites. Malar. J. *21*, 247. https://doi.org/10.1186/s12936-022-04261-z.

34. Chen, Z.W. (2011). Immune biology of Ag-specific γδ T cells in infections. Cell. Mol. Life Sci. *68*, 2409–2417. https://doi.org/10.1007/s00018-011-0703-9.

35. Davey, M.S., Willcox, C.R., Hunter, S., Kasatskaya, S.A., Remmerswaal, E.B.M., Salim, M., Mohammed, F., Bemelman, F.J., Chudakov, D.M., Oo, Y.H., and Willcox, B.E. (2018). The human Vδ2+ T-cell compartment comprises distinct innate-like Vγ9+ and adaptive Vγ9- subsets. Nat. Commun. *9*, 1760. https://doi.org/10.1038/s41467-018-04076-0.

36. Davey, M.S., Willcox, C.R., Hunter, S., Oo, Y.H., and Willcox, B.E. (2018). Vδ2+ T cells—two subsets for the Price of One. Front. Immunol. *9*, 2106. https://doi.org/10.3389/fimmu.2018.02106.

37. Caccamo, N., Dieli, F., Wesch, D., Jomaa, H., and Eberl, M. (2006). Sex-specific phenotypical and functional differences in peripheral human Vγ9/Vδ2 T cells. J. Leukoc. Biol. *79*, 663–666. https://doi.org/10.1189/jlb.1105640.

38. Dieli, F., Poccia, F., Lipp, M., Sireci, G., Caccamo, N., Di Sano, C., and Salerno, A. (2003). Differentiation of effector/memory Vδ2 T cells and Migratory routes in lymph nodes or Inflammatory sites. J. Exp. Med. *198*, 391–397. https://doi.org/10.1084/jem.20030235.

39. Ram, D.R., Lucar, O., Hueber, B., and Reeves, R.K. (2019). Simian immunodeficiency virus infection Modulates CD94 + (KLRD1 +) NK cells in rhesus macaques. J. Virol. *93*, e00731-19. https://doi.org/10.1128/jvi.00731-19.

40. Khairallah, C., Chu, T.H., and Sheridan, B.S. (2018). Tissue Adaptations of memory and tissue-resident gamma delta T cells. Front. Immunol. *9*, 2636. https://doi.org/10.3389/fimmu.2018.02636.

41. McMurray, J.L., von Borstel, A., Taher, T.E., Syrimi, E., Taylor, G.S., Sharif, M., Rossjohn, J., Remmerswaal, E.B.M., Bemelman, F.J., Vieira Braga, F.A., et al. (2022). Transcriptional profiling of human Vδ1 T cells reveals a pathogen-driven adaptive differentiation program. Cell Rep. *39*, 110858. https://doi.org/10.1016/j.celrep.2022.110858.

42. Alonzo, E.S., and Sant'Angelo, D.B. (2011). Development of PLZF-expressing innate T cells. Curr. Opin. Immunol. *23*, 220–227. https://doi.org/10.1016/j.coi.2010.12.016.

43. Eidson, M., Wahlstrom, J., Beaulieu, A.M., Zaidi, B., Carsons, S.E., Crow, P.K., Yuan, J., Wolchok, J.D., Horsthemke, B., Wieczorek, D., and Sant'Angelo, D.B. (2011). Altered development of NKT cells, γδ T cells, CD8 T cells and NK cells in a PLZF Deficient Patient. PLoS One *6*, e24441. https://doi.org/10.1371/journal.pone.0024441.

44. Hunter, S., Willcox, C.R., Davey, M.S., Kasatskaya, S.A., Jeffery, H.C., Chudakov, D.M., Oo, Y.H., and Willcox, B.E. (2018). Human liver infiltrating γδ T cells are composed of clonally expanded circulating and tissue-resident populations. J. Hepatol. *69*, 654–665. https://doi.org/10.1016/j.jhep.2018.05.007.

45. Zakeri, N., Hall, A., Swadling, L., Pallett, L.J., Schmidt, N.M., Diniz, M.O., Kucykowicz, S., Amin, O.E., Gander, A., Pinzani, M., et al. (2022). Characterisation and induction of tissue-resident gamma delta T-cells to target hepatocellular carcinoma. Nat. Commun. *13*, 1372. https://doi.org/10.1038/s41467-022-29012-1.

46. Caccamo, N., Battistini, L., Bonneville, M., Poccia, F., Fournié, J.J., Meraviglia, S., Borsellino, G., Kroczek, R.A., La Mendola, C., Scotet, E., et al. (2006). CXCR5 identifies a subset of Vγ9Vδ2 T cells which Secrete IL-4 and IL-10 and help B cells for antibody production. J. Immunol. *177*, 5290–5295.

https://doi.org/10.4049/jimmunol.177.8.5290.

47. Zhu, X., and Zhu, J. (2020). CD4 T helper cell subsets and related human immunological Disorders. Int. J. Mol. Sci. *21*, 8011. https://doi.org/10.3390/ijms21218011.

48. Gioulbasani, M., Galaras, A., Grammenoudi, S., Moulos, P., Dent, A.L., Sigvardsson, M., Hatzis, P., Kee, B.L., and Verykokakis, M. (2020). The transcription factor BCL-6 controls early development of innate-like T cells. Nat. Immunol. *21*, 1058–1069. https://doi.org/10.1038/s41590-020-0737-y.

49. Kroca, M., Johansson, A., Sjöstedt, A., and Tärnvik, A. (2001). Vγ9Vδ2 T cells in human Legionellosis. Clin. Diagn. Lab. Immunol. *8*, 949–954. https://doi.org/10.1128/cdli.8.5.949-954.2001.

50. Tyler, C.J., McCarthy, N.E., Lindsay, J.O., Stagg, A.J., Moser, B., and Eberl, M. (2017). Antigen-presenting human γδ T cells promote intestinal CD4+ T cell expression of IL-22 and mucosal Release of Calprotectin. J. Immunol. *198*, 3417–3425. https://doi.org/10.4049/jimmunol.1700003.

51. McCarthy, N.E., Bashir, Z., Vossenkämper, A., Hedin, C.R., Giles, E.M., Bhattacharjee, S., Brown, S.G., Sanders, T.J., Whelan, K., MacDonald, T.T., et al. (2013). Proinflammatory Vδ2+ T cells populate the human intestinal mucosa and enhance IFN-γ production by colonic αβ T cells. J. Immunol. *191*, 2752–2763. https://doi.org/10.4049/jimmunol.1202959.

52. Ness-Schwickerath, K.J., Jin, C., and Morita, C.T. (2010). Cytokine Requirements for the differentiation and expansion of IL-17A– and IL-22–Producing human Vγ2Vδ2 T cells. J. Immunol. *184*, 7268–7280. https://doi.org/10.4049/jimmunol.1000600.

53. Sicard, H., Ingoure, S., Luciani, B., Serraz, C., Fournié, J.J., Bonneville, M., Tiollier, J., and Romagné, F. (2005). In vivo Immunomanipulation of Vγ9Vδ2 T cells with a Synthetic phosphoantigen in a preclinical nonhuman primate model. J. Immunol. *175*, 5471–5480. https://doi.org/10.4049/jimmunol.175.8.5471.

54. El-Sherbiny, Y.M., Meade, J.L., Holmes, T.D., McGonagle, D., Mackie, S.L., Morgan, A.W., Cook, G., Feyler, S., Richards, S.J., Davies, F.E., et al. (2007). The Requirement for DNAM-1, NKG2D, and NKp46 in the natural killer cell-mediated killing of myeloma cells. Cancer Res. *67*, 8444–8449. https://doi.org/10.1158/0008-5472.can-06-4230.

55. Zhang, Z., Wu, N., Lu, Y., Davidson, D., Colonna, M., and Veillette, A. (2015). DNAM-1 controls NK cell activation via an ITT-like motif. J. Exp. Med. *212*, 2165–2182. https://doi.org/10.1084/jem.20150792.

56. Meraviglia, S., Eberl, M., Vermijlen, D., Todaro, M., Buccheri, S., Cicero, G., La Mendola, C., Guggino, G., D'Asaro, M., Orlando, V., et al. (2010). In vivo manipulation of Vgamma9Vdelta2 T cells with zoledronate and low-dose interleukin-2 for immunotherapy of advanced breast cancer patients. Clin. Exp. Immunol. *161*, 290–297. https://doi.org/10.1111/j.1365-2249.2010.04167.x.

57. Lang, J.M., Kaikobad, M.R., Wallace, M., Staab, M.J., Horvath, D.L., Wilding, G., Liu, G., Eickhoff, J.C., McNeel, D.G., and Malkovsky, M. (2011). Pilot trial of interleukin-2 and zoledronic acid to augment γδ T cells as treatment for patients with refractory renal cell carcinoma. Cancer Immunol. Immunother. *60*, 1447–1460. https://doi.org/10.1007/s00262-011-1049-8.

58. Kunzmann, V., Smetak, M., Kimmel, B., Weigang-Koehler, K., Goebeler, M., Birkmann, J., Becker, J., Schmidt-Wolf, I.G.H., Einsele, H., and Wilhelm, M. (2012). Tumor-promoting versus tumor-antagonizing roles of γδ T cells in cancer immunotherapy: results from a Prospective phase I/II trial. J. Immunother. *35*, 205–213. https://doi.org/10.1097/cji.0b013e318245bb1e.

59. Pressey, J.G., Adams, J., Harkins, L., Kelly, D., You, Z., and Lamb, L.S. (2016). In vivo expansion and activation of γδ T cells as immunotherapy for refractory neuroblastoma: a phase 1 study. Medicine *95*, e4909. https://doi.org/10.1097/md.0000000000004909.

60. Hintz, M., Reichenberg, A., Altincicek, B., Bahr, U., Gschwind, R.M., Kollas, A.-K., Beck, E., Wiesner, J., Eberl, M., and Jomaa, H. (2001). Identification of (E)-4-hydroxy-3-methyl-but-2-enyl pyrophosphate as a major activator for human γδ T cells in Escherichia coli. FEBS Lett. *509*, 317–322. https://doi.org/10.1016/s0014-5793(01)03191-x.

61. De Gassart, A., Le, K.-S., Brune, P., Agaugué, S., Sims, J., Goubard, A., Castellano, R., Joalland, N., Scotet, E., Collette, Y., et al. (2021). Development of ICT01, a first-in-class, anti-BTN3A antibody for activating Vγ9Vδ2 T cell–mediated antitumor immune response. Sci. Transl. Med. *13*, eabj0835. https://doi.org/10.1126/scitranslmed.abj0835.

62. Sireci, G., Espinosa, E., Sano, C., Dieli, F., Fournié, J.J., and Salerno, A. (2001). Differential activation of human γ δ cells by nonpeptide phosphoantigens. Eur. J. Immunol. *31*, 1628–1635. https://doi.org/10.1002/1521-4141.

63. Casetti, R., Perretta, G., Taglioni, A., Mattei, M., Colizzi, V., Dieli, F., D'Offizi, G., Malkovsky, M., and Poccia, F. (2005). Drug-induced expansion and differentiation of Vγ9Vδ2 T cells in vivo: the role of exogenous IL-2. J. Immunol. *175*, 1593–1598. https://doi.org/10.4049/jimmunol.175.3.1593.

64. Cazzetta, V., Bruni, E., Terzoli, S., Carenza, C., Franzese, S., Piazza, R., Marzano, P., Donadon, M., Torzilli, G., Cimino, M., et al. (2021). NKG2A expression identifies a subset of human Vδ2 T cells exerting the highest antitumor effector functions. Cell Rep. *37*, 109871. https://doi.org/10.1016/j.celrep.2021.109871.

65. Vyborova, A., Beringer, D.X., Fasci, D., Karaiskaki, F., van Diest, E., Kramer, L., de Haas, A., Sanders, J., Janssen, A., Straetemans, T., et al. (2020). γ9δ2T cell diversity and the receptor interface with tumor cells. J. Clin. Invest. *130*, 4637–4651. https://doi.org/10.1172/jci132489.

66. Willcox, C.R., Davey, M.S., and Willcox, B.E. (2018). Development and selection of the human Vγ9Vδ2+ T-cell repertoire. Front. Immunol. *9*, 1501. https://doi.org/10.3389/fimmu.2018.01501.

67. MacDougall, A., Enders, P., Hatfield, G., Pauza, D., and Rakasz, E. (2001). Vγ2 TCR repertoire overlap in different anatomical compartments of healthy, unrelated rhesus macaques. J. Immunol. *166*, 2296–2302. https://doi.org/10.4049/jimmunol.166.4.2296.

68. Juno, J.A., Wragg, K.M., Amarasena, T., Meehan, B.S., Mak, J.Y.W., Liu, L., Fairlie, D.P., McCluskey, J., Eckle, S.B.G., and Kent, S.J. (2019). MAIT cells upregulate α4β7 in response to acute simian immunodeficiency virus/simian hiv infection but are resistant to peripheral depletion in pigtail macaques. J. Immunol. *202*, 2105–2120. https://doi.org/10.4049/jimmunol.1801405.

69. Bennouna, J., Levy, V., Sicard, H., Senellart, H., Audrain, M., Hiret, S., Rolland, F., Bruzzoni-Giovanelli, H., Rimbert, M., Galéa, C., et al. (2010). Phase I study of bromohydrin pyrophosphate (BrHPP, IPH 1101), a Vγ9Vδ2 T lymphocyte agonist in patients with solid tumors. Cancer Immunol. Immunother. *59*, 1521–1530. https://doi.org/10.1007/s00262-010-0879-0.

70. Spencer, C.T., Abate, G., Sakala, I.G., Xia, M., Truscott, S.M., Eickhoff, C.S., Linn, R., Blazevic, A., Metkar, S.S., Peng, G., et al. (2013). Granzyme A produced by γ9δ2 T cells induces human macrophages to inhibit growth of an intracellular pathogen. PLoS Pathog. *9*, e1003119. https://doi.org/10.1371/journal.ppat.1003119.

71. Wang, C., Kang, S.G., Lee, J., Sun, Z., and Kim, C.H. (2009). The roles of CCR6 in migration of Th17 cells and regulation of effector T-cell balance in the gut. Mucosal Immunol. *2*, 173–183. https://doi.org/10.1038/mi.2008.84.

72. Lee, A.Y.S., and Körner, H. (2019). The CCR6-CCL20 axis in humoral immunity and T-B cell immunobiology. Immunobiology *224*, 449–454. https://doi.org/10.1016/j.imbio.2019.01.005.

73. WILLIAMS, I.R. (2006). CCR6 and CCL20. Ann. N. Y. Acad. Sci. *1072*, 52–61. https://doi.org/10.1196/annals.1326.036.

74. Meitei, H.T., Jadhav, N., and Lal, G. (2021). CCR6-CCL20 axis as a therapeutic target for autoimmune diseases. Autoimmun. Rev. *20*, 102846. https://doi.org/10.1016/j.autrev.2021.102846.

75. Zhang, Y., Roth, T.L., Gray, E.E., Chen, H., Rodda, L.B., Liang, Y., Ventura, P., Villeda, S., Crocker, P.R., and Cyster, J.G. (2016). Migratory and adhesive cues controlling innate-like lymphocyte surveillance of the pathogen-exposed surface of the lymph node. Elife *5*, e18156. https://doi.org/10.7554/elife.18156.

76. Mehta, H., Lett, M.J., Klenerman, P., and Filipowicz Sinnreich, M. (2022). MAIT cells in liver inflammation and fibrosis. Semin. Immunopathol. *44*, 429–444. https://doi.org/10.1007/s00281-022-00949-1.

77. Affò, S., Rodrigo-Torres, D., Blaya, D., Morales-Ibanez, O., Coll, M., Millán, C., Altamirano, J., Arroyo, V., Caballería, J., Bataller, R., et al. (2015). Chemokine receptor Ccr6 deficiency alters hepatic Inflammatory cell recruitment and promotes liver inflammation and fibrosis. PLoS One *10*, e0145147. https://doi.org/10.1371/journal.pone.0145147.

78. Facco, M., Baesso, I., Miorin, M., Bortoli, M., Cabrelle, A., Boscaro, E., Gurrieri, C., Trentin, L., Zambello, R., Calabrese, F., et al. (2007). Expression and role of CCR6/CCL20 chemokine axis in pulmonary sarcoidosis. J. Leukoc. Biol. *82*, 946–955. https://doi.org/10.1189/jlb.0307133.

79. Ito, T., Carson, W.F., Cavassani, K.A., Connett, J.M., and Kunkel, S.L. (2011). CCR6 as a mediator of immunity in the lung and gut. Exp. Cell Res. *317*, 613–619. https://doi.org/10.1016/j.yexcr.2010.12.018.

80. Workalemahu, G., Wang, H., Puan, K.-J., Nada, M.H., Kuzuyama, T., Jones, B.D., Jin, C., and Morita, C.T. (2014). Metabolic engineering of Salmonella vaccine bacteria to boost human Vγ2Vδ2 T cell immunity. J. Immunol. *193*, 708–721. https://doi.org/10.4049/jimmunol.1302746.

81. Hao, J., Wu, X., Xia, S., Li, Z., Wen, T., Zhao, N., Wu, Z., Wang, P., Zhao, L., and Yin, Z. (2010). Current progress in γδ T-cell biology. Cell. Mol. Immunol. *7*, 409–413. https://doi.org/10.1038/cmi.2010.50.

82. Spencer, C.T., Abate, G., Blazevic, A., and Hoft, D.F. (2008). Only a subset of phosphoantigen-responsive γ9δ2 T cells mediate protective tuberculosis immunity. J. Immunol. *181*, 4471–4484. https://doi.org/10.4049/jimmunol.181.7.4471.

83. Fichtner, A.S., Bubke, A., Rampoldi, F., Wilharm, A., Tan, L., Steinbrück, L., Schultze-Florey, C., von Kaisenberg, C., Prinz, I., Herrmann, T., and Ravens, S. (2020). TCR repertoire analysis reveals phosphoantigen-induced polyclonal proliferation of Vγ9Vδ2 T cells in neonates and adults. J. Leukoc. Biol. *107*, 1023–1032. https://doi.org/10.1002/jlb.1ma0120-427rr.

84. Shimonkevitz, R., Colburn, C., Burnham, J.A., Murray, R.S., and Kotzin, B.L. (1993). Clonal expansions of activated gamma/delta T cells in recent-onset multiple sclerosis. Proc. Natl. Acad. Sci. USA *90*, 923–927. https://doi.org/10.1073/pnas.90.3.923.

85. Huang, D., Chen, C.Y., Zhang, M., Qiu, L., Shen, Y., Du, G., Zhou, K., Wang, R., and Chen, Z.W. (2012). Clonal immune responses of Mycobacterium-specific γδ T cells in tuberculous and non-tuberculous tissues during M. tuberculosis infection. PLoS One *7*, e30631. https://doi.org/10.1371/journal.pone.0030631.

86. Vu, M.N., Kelly, H.G., Tan, H.X., Juno, J.A., Esterbauer, R., Davis, T.P., Truong, N.P., Wheatley, A.K., and Kent, S.J. (2021). Hemagglutinin functionalized liposomal vaccines enhance germinal center and follicular helper T cell immunity. Adv. Healthc. Mater. *10*, 2002142. https://doi.org/10.1002/adhm.202002142.

87. Li, X., Valdes, S.A., Alzhrani, R.F., Hufnagel, S., Hursting, S.D., and Cui, Z. (2019). Zoledronic acid-containing nanoparticles with minimum premature release show enhanced activity against extraskeletal tumor. ACS Appl. Mater. Interfaces *11*, 7311–7319. https://doi.org/10.1021/acsami.8b16588.

88. Rakasz, E., MacDougall, A.V., Zayas, M.T., Helgelund, J.L., Ruckward, T.J., Hatfield, G., Dykhuizen, M., Mitchen, J.L., Evans, P.S., and Pauza, C.D. (2000). γδ T cell receptor repertoire in blood and colonic mucosa of rhesus macaques. J. Med. Primatol. *29*, 387–396. https://doi.org/10.1111/j.1600-0684.2000.290602.x.

89. Bolotin, D.A., Poslavsky, S., Mitrophanov, I., Shugay, M., Mamedov, I.Z., Putintseva, E.V., and Chudakov, D.M. (2015). MiXCR: software for comprehensive adaptive immunity profiling. Nat. Methods *12*, 380–381. https://doi.org/10.1038/nmeth.3364.

90. Gu, Z., Gu, L., Eils, R., Schlesner, M., and Brors, B. (2014). circlize implements and enhances circular visualization in R. Bioinformatics *30*, 2811–2812. https://doi.org/10.1093/bioinformatics/btu393.

91. Brunson, J. (2020). ggalluvial: Layered Grammar for Alluvial Plots. J. Open Source Softw. *5*, 2017. https://doi.org/10.21105/joss.02017.

92. Bodenhofer, U., Bonatesta, E., Horejš-Kainrath, C., and Hochreiter, S. (2015). msa: an R package for multiple sequence alignment. Bioinformatics *31*, 3997–3999. https://doi.org/10.1093/bioinformatics/btv494.

93. R Core Team (2022). R: A language and environment for statistical computing (Vienna, Austria: R Foundation for Statistical Computing). https://www.R-project.org/.

94. Wickham, H., Averick, M., Bryan, J., Chang, W., McGowan, L., François, R., Grolemund, G., Hayes, A., Henry, L., Hester, J., et al. (2019). Welcome to the Tidyverse. J. Open Source Softw. *4*, 1686. https://doi.org/10.21105/joss.01686.

95. Conway, J.R., Lex, A., and Gehlenborg, N. (2017). UpSetR: an R package for the visualization of intersecting sets and their properties. Bioinformatics *33*, 2938–2940. https://doi.org/10.1093/bioinformatics/btx364.

96. Oksanen, J., Simpson, G.L., Blanchet, F.G., Kindt, R., Legendre, P., Minchin P.R., O'Hara, R.B., Solymos, P., Stevens, M.H., Szoecs, E., et al., (2022). vegan: Community Ecology Package. https://CRAN.R-project.org/package=vegan.

97. Parsons, M.S., Lee, W.S., Kristensen, A.B., Amarasena, T., Khoury, G., Wheatley, A.K., Reynaldi, A., Wines, B.D., Hogarth, P.M., Davenport, M.P., and Kent, S.J. (2019). Fc-dependent functions are redundant to efficacy of anti-HIV antibody PGT121 in macaques. J. Clin. Invest. *129*, 182–191. https://doi.org/10.1172/jci122466.

98. Li, J., Ahmet, F., Sullivan, L.C., Brooks, A.G., Kent, S.J., De Rose, R., Salazar, A.M., Reis e Sousa, C., Shortman, K., Lahoud, M.H., et al. (2015). Antibodies targeting Clec9A promote strong humoral immunity without adjuvant in mice and non-human primates. Eur. J. Immunol. *45*, 854–864. https://doi.org/10.1002/eji.201445127.

99. Parsons, M.S., Lloyd, S.B., Lee, W.S., Kristensen, A.B., Amarasena, T., Center, R.J., Keele, B.F., Lifson, J.D., LaBranche, C.C., Montefiori, D., et al. (2017). Partial efficacy of a broadly neutralizing antibody against cell-associated SHIV infection. Sci. Transl. Med. *9*, eaaf1483. https://doi.org/10.1126/scitranslmed.aaf1483.

100. Khanna, M., Jackson, R.J., Alcantara, S., Amarasena, T.H., Li, Z., Kelleher, A.D., Kent, S.J., and Ranasinghe, C. (2019). Mucosal and systemic SIV-specific cytotoxic CD4 + T cell hierarchy in protection following intranasal/intramuscular recombinant pox-viral vaccination of pigtail macaques. Sci. Rep. *9*, 5661. https://doi.org/10.1038/s41598-019-41506-5.

101. Barber-Axthelm, I.M., Kelly, H.G., Esterbauer, R., Wragg, K.M., Gibbon, A.M., Lee, W.S., Wheatley, A.K., Kent, S.J., Tan, H.-X., and Juno, J.A. (2021). Coformulation with tattoo ink for immunological assessment of vaccine immunogenicity in the draining lymph node. J. Immunol. *207*, 735–744. https://doi.org/10.4049/jimmunol.2001299.

102. Kelly, H.G., Tan, H.-X., Juno, J.A., Esterbauer, R., Ju, Y., Jiang, W., Wimmer, V.C., Duckworth, B.C., Groom, J.R., Caruso, F., et al. (2020). Self-assembling influenza nanoparticle vaccines drive extended germinal center activity and memory B cell maturation. Jci Insight *5*, e136653. https://doi.org/10.1172/jci.insight.136653.

103. Dash, P., McClaren, J.L., Oguin, T.H., Rothwell, W., Todd, B., Morris, M.Y., Becksfort, J., Reynolds, C., Brown, S.A., Doherty, P.C., and Thomas, P.G. (2011). Paired analysis of TCRα and TCRβ chains at the single-cell level in mice. J. Clin. Invest. *121*, 288–295. https://doi.org/10.1172/jci44752.

104. Wang, G.C., Dash, P., McCullers, J.A., Doherty, P.C., and Thomas, P.G. (2012). T cell receptor αβ diversity inversely correlates with pathogen-specific antibody levels in human cytomegalovirus infection. Sci. Transl. Med. *4*, 128ra42. https://doi.org/10.1126/scitranslmed.3003647.

105. Rowntree, L.C., Petersen, J., Juno, J.A., Chaurasia, P., Wragg, K., Koutsakos, M., Hensen, L., Wheatley, A.K., Kent, S.J., Rossjohn, J., et al. (2021). SARS-CoV-2-specific CD8+ T-cell responses and TCR signatures in the context of a prominent HLA-A*24:02 allomorph.

Immunol. Cell Biol. *99*, 990–1000. https://doi.org/10.1111/imcb.12482.

106. Valkenburg, S.A., Josephs, T.M., Clemens, E.B., Grant, E.J., Nguyen, T.H.O., Wang, G.C., Price, D.A., Miller, A., Tong, S.Y.C., Thomas, P.G., et al. (2016). Molecular basis for universal HLA-A*0201–restricted CD8+ T-cell immunity against influenza viruses. Proc. Natl. Acad. Sci. USA *113*, 4440–4445. https://doi.org/10.1073/pnas.1603106113.

107. Nguyen, T.H.O., Rowntree, L.C., Pellicci, D.G., Bird, N.L., Handel, A., Kjer-Nielsen, L., Kedzierska, K., Kotsimbos, T.C., and Mifsud, N.A. (2014). Recognition of distinct Cross-reactive virus-specific CD8+ T cells reveals a unique TCR Signature in a clinical setting. J. Immunol. *192*, 5039–5049. https://doi.org/10.4049/jimmunol.1303147.

108. Venturi, V., Kedzierska, K., Turner, S.J., Doherty, P.C., and Davenport, M.P. (2007). Methods for comparing the diversity of samples of the T cell receptor repertoire. J. Immunol. Methods *321*, 182–195. https://doi.org/10.1016/j.jim.2007.01.019.

STAR★METHODS

KEY RESOURCES TABLE

REAGENT or RESOURCE	SOURCE	IDENTIFIER
Antibodies		
Mouse monoclonal anti-Bcl6 Alexa Fluor 647 conjugated (clone: IG191E/A8)	BioLegend	Cat# 648306; RRID: AB_2565299
Mouse monoclonal anti-CD3 Alexa Fluor 700 conjugated (clone: SP34-2)	BD Biosciences	Cat# 557917; RRID: AB_396938
Mouse monoclonal anti-CD3 BUV805 conjugated (clone: SP34-2)	BD Biosciences	Cat# 742053; RRID: AB_2871342
Mouse monoclonal anti-CD20 BUV805 conjugated (clone: 2H7)	BD Biosciences	Cat# 612905; RRID: AB_2870192
Mouse monoclonal anti-CD20 BV510 conjugated (clone: 2H7)	BD Biosciences	Cat# 563067; RRID: AB_2737985
Mouse monoclonal anti-CD20 PE-CF594 conjugated (clone: 2H7)	BD Biosciences	Cat# 562295; RRID: AB_11153322
Mouse monoclonal anti-CD26 unconjugated (clone: clone5)	In house	N/A
Mouse monoclonal anti-CD28 BV711 conjugated (clone: CD28.2)	BD Biosciences	Cat# 563131; RRID: AB_2738020
Mouse monoclonal anti-CD45 BUV395 conjugated (clone: D058-1283)	BD Biosciences	Cat# 564099; RRID: AB_2738591
Mouse monoclonal anti-CD45 PE-Cy7 conjugated (clone: D058-1283)	BD Biosciences	Cat# 561294; RRID: AB_10612014
Mouse monoclonal anti-CD69 APC/Fire 750 conjugated (clone: FN50)	BioLegend	Cat# 310946; RRID: AB_2616709
Mouse monoclonal anti-CD94 APC conjugated (clone: HP-3D9)	BD Biosciences	Cat# 559876; RRID: AB_398679
Mouse monoclonal anti-CD95 BUV737 conjugated (clone: DX2)	BD Biosciences	Cat# 612790; RRID: AB_2870117
Mouse monoclonal anti-CD95 PE-Cy7 conjugated (clone: DX2)	BD Biosciences	Cat# 561633; RRID: AB_10894384
Mouse monoclonal anti-CD159a (NKG2A) APC conjugated (clone: Z199)	Beckman Coulter	Cat# A60797; RRID: AB_10643105
Mouse monoclonal anti-CD183 (CXCR3) Alexa Fluor 647 conjugated (clone: G025H7)	BioLegend	Cat# 353712; RRID: AB_10962948
Mouse monoclonal anti-CD183 (CXCR3) Alexa Fluor 700 conjugated (clone: G025H7)	BioLegend	Cat# 353742; RRID: AB_2616920
Mouse monoclonal anti-CD183 (CXCR3) PE-Dazzle594 (clone: G025H7)	BioLegend	Cat# 353736; RRID:AB_2564288
Mouse monoclonal anti-CD185 (CXCR5) PE-eFluor610 conjugated (clone: MU5UBEE)	Thermo Fisher Scientific	Cat# 61-9185-42; RRID: AB_2574677
Rat monoclonal anti-CD195 (CCR5) BV421 conjugated (clone: J418F1)	BioLegend	Cat# 359118; RRID: AB_2563577
Mouse monoclonal anti-CD196 (CCR6) BV785 conjugated (clone: G034E3)	BioLegend	Cat# 353422; RRID: AB_2563660
Mouse monoclonal anti-CD218 (IL-18Rα) PE-Vio770 conjugated (clone: H44)	Miltenyi Biotec	Cat# 130-101-723; RRID: AB_2656352
Mouse monoclonal anti-CD226 (DNAM-1) BV605 conjugated (clone: 11A8)	BioLegend	Cat# 338324; RRID: AB_2721543
Mouse monoclonal anti-CD326 (Ep-CAM) PE-CF594 conjugated (clone: EBA-1)	BD Biosciences	Cat# 565399; RRID: AB_2739219
Mouse monoclonal anti-eomes PerCP-eFluor710 conjugated (clone: WD1928)	Thermo Fisher Scientific	Cat# 46-4877-42; RRID: AB_2573759

(*Continued on next page*)

Continued

REAGENT or RESOURCE	SOURCE	IDENTIFIER
Rat monoclonal anti-GM-CSF BV421 conjugated (clone: BVD2-21C11)	BD Biosciences	Cat# 562930; RRID: AB_2737899
Mouse monoclonal anti-granzyme B BV510 conjugated (clone: GB11)	BD Biosciences	Cat# 563388; RRID: AB_2738174
Mouse monoclonal anti-IFNγ BUV395 conjugated (clone: B27)	BD Biosciences	Cat# 563563; RRID: AB_2738277
Mouse monoclonal anti-IL-17A BV605 conjugated (clone: BL168)	BioLegend	Cat# 512326; RRID: AB_2563887
Mouse monoclonal anti-PLZF PE-CF594 conjugated (clone: R17-809)	BD Biosciences	Cat# 565738; RRID: AB_2739339
Mouse monoclonal anti-T-bet BV421 conjugated (clone: 4B10)	BioLegend	Cat# 644816; RRID: AB_10959653
Mouse monoclonal anti-TCR Vδ1 PE-Cy7 conjugated (clone: TS8.2)	Thermo Fisher Scientific	Cat# 25-5679-42; RRID: AB_2762454
Mouse monoclonal anti-TCR Vδ2 FITC conjugated (clone: 15D)	Thermo Fisher Scientific	Cat# TCR2732; RRID:AB_417095
Mouse monoclonal anti-TCR Vδ2 unconjugated (clone: 15D)	Thermo Fisher Scientific	Cat# TCR1732; RRID: AB_417090
Mouse monoclonal anti-TCR Vγ9 FITC conjugated (clone: 7A5)	Thermo Fisher Scientific	Cat# TCR2720; RRID: AB_417094
Mouse monoclonal anti-TNFα APC-Cy7 conjugated (clone: MAb11)	BioLegend	Cat# 502944; RRID: AB_2562870
Goat polyclonal anti-mouse IgG (H + L) cross-adsorbed secondary PE conjugated	Thermo Fisher Scientific	Cat# P-852; RRID: AB_2539848
Biological samples		
Healthy human whole blood	University of Melbourne, Department of Microbiology and Immunology	N/A
Chemicals, peptides, and recombinant proteins		
Anti-PE MicroBeads	Miltenyi Biotec	Cat# 130-048-801
Cytofix	BD Biosciences	Cat# 554655
Cytofix/cytoperm kit	BD Biosciences	Cat# 554714
dNTP mix	Meridian Bioscience	Cat# BIO-39053
(E)-1-Hydroxy-2-methyl-2-butenyl 4-pyrophosphate lithium salt (HMB-PP)	Sigma Aldrich	Cat# 95098; CAS# 396726-03-7
Ficoll-Paque Plus	Sigma Aldrich	Cat# GE17-1440-03
GolgiPlug	BD Biosciences	Cat# 555029
GolgiStop	BD Biosciences	Cat# 554724
Igepal	Sigma Aldrich	Cat# I8896; CAS# 9002-93-1
Ionomycin	Sigma Aldrich	Cat# 13909; EC# 200-664-3
Isopentenyl pyrophosphate trilithium salt (IPP)	Sigma Aldrich	Cat# 00297; CAS# 18687-43-9
Live/dead fixable aqua dead cell stain	Thermo Fisher Scientific	Cat# L34957
Live/dead fixable blue dead cell stain	Thermo Fisher Scientific	Cat# L34962
Live/dead fixable green dead cell stain	Thermo Fisher Scientific	Cat# L34970
Phorbol 12-Myristate 13-Acetate	Abcam	CAT# ab120297; CAS# 16561-29-8
Random hexamer primer	Meridian Bioscience	Cat# BIO-38028
Recombinant human IL-2	Peprotech	Cat# 200-02; Accession# P60568
Recombinant rhesus macaque IL-12	R and D Systems	Cat# 3216-RL-025; Accession# P48095 and NP_001038199
Recombinant rhesus macaque IL-18	R and D Systems	Cat# 2548-RM-025; Accession# AAK13416
RNasin Plus Ribonuclease Inhibitor	Promega	Cat# N2615

(*Continued on next page*)

Continued

REAGENT or RESOURCE	SOURCE	IDENTIFIER
Streptavidin PE-TR	Thermo Fisher Scientific	Cat# SA1017
SYBR Safe DNA gel stain	Thermo Fisher Scientific	Cat# S33102
Transcription buffer staining kit	BD Biosciences	Cat# 562574
Zoledronic acid monohydrate (Zol)	Sigma Aldrich	Cat# SML0223; CAS# 165800-06-6
Critical commercial assays		
Biotinylation Kit / Biotin Conjugation Kit (Fast, Type A)	Abcam	Cat# ab201795
HotStarTaq Plus DNA Polymerase	Qiagen	Cat# 203609
SuperScript III Reverse Transcriptase	Thermo Fisher Scientific	Cat# 18080044
Deposited data		
Aligned, single-cell TCRG/TCRD sequences	This paper	Mendeley Data: https://doi.org/10.17632/bpwtp95rpw.1
Experimental models: Organisms/strains		
Pigtail macaques (*Macaca nemestrina*)	Australian National Macaque Breeding Colony	N/A
Oligonucleotides		
CAT CTA TGG CCC TGG TTT CA	Integrated DNA Technologies	Rakasz et al.[88]; Fwd, macTCRDV2- External
TGG CAG TCA AGA GAA AAT TG	Integrated DNA Technologies	Rakasz et al.[88]; Rev, macTCRDC- External
AGA CCT GGT GAA GTC ATA C	Integrated DNA Technologies	Rakasz et al.[88]; Fwd, macTCRGV9- External
GTT GCT CTT CTT TTC TTG CC	Integrated DNA Technologies	Rakasz et al.[88]; Rev, macTCRGC- External
CAG AGA GAG ATG AAG GGT CTT AC	Integrated DNA Technologies	Fwd, macTCRDV2- Internal
CAC TGG GAG AGA CGA CAA TAG	Integrated DNA Technologies	Rev, macTCRDC- Internal
CCT GGT GAA GTC ATA CAG TTC C	Integrated DNA Technologies	macTCRGV9- Internal
AAT AGT GGG CTT GGG TGA AAT A	Integrated DNA Technologies	macTCRGC- Internal
Software and algorithms		
Code for TCR sequence processing and analysis	This paper	GitHub: https://github.com/BarberAxthelm/Vd2-Vg9_TCR_Analysis
BD FACSDiva	BD Biosciences	N/A
Biorender	Biorender	https://biorender.com/
FlowJo (v10.8.1)	FlowJo, LLC, BD Biosciences	https://www.flowjo.com/
MiXCR (v3.0.13)	Bolotin et al.[89]	https://docs.milaboratories.com/
Prism (v9.4.1)	GraphPad	https://www.graphpad.com/scientific-software/prism/
RStudio (v4.1.3)	RStudio, PBC	https://www.rstudio.com/
circlize (v0.4.15)	Gu et al.[90]	https://jokergoo.github.io/circlize_book/book/
ggalluvial (v0.12.3)	Brunson[91]	https://corybrunson.github.io/ggalluvial/
msa (v1.26.0)	Bodenhofer et al.[92]	http://bioconductor.org/packages/release/bioc/html/msa.html
Parallel	R Core Team[93]	https://www.R-project.org/
Tidyverse (v1.3.1)	Wickham et al.[94]	https://www.tidyverse.org/
UpSetR (v1.4.0)	Conway et al.[95]	https://cran.r-project.org/web/packages/UpSetR/index.html
vegan (v2.6-2)	Jari Oksanen, et al.[96]	https://CRAN.R-project.org/package=vegan

(*Continued on next page*)

Continued

REAGENT or RESOURCE	SOURCE	IDENTIFIER
Other		
BD FACSAria III cell sorter	BD Biosciences	N/A
BD LSRFortessa cell analyzer	BD Biosciences	N/A
CELL-DYN Emerald Hematology Analyzer	Abbott Laboratories	N/A

RESOURCE AVAILABILITY

Lead contact

Further information and requests for resources and reagents should be directed to and will be fulfilled by the lead contact, Jennifer Juno (jennifer.juno@unimelb.edu.au).

Materials availability

This study did not generate new unique reagents.

Data and code availability

Paired, aligned, single-cell TCRG/TCRD sequences, and associated flow cytometry sorting data, has been deposited at Mendeley Data, and is publicly available as of the date of publication (Mendeley Data: https://doi.org/10.17632/bpwtp95rpw.1).All other data reported in this paper will be shared by the lead contact upon request.

All original code has been deposited at GitHub (GitHub: https://github.com/BarberAxthelm/Vd2-Vg9_TCR_Analysis) and is publicly available as of the date of publication.

Any additional information required to re-analyze the data reported in this paper is available from the lead contact upon request.

EXPERIMENTAL MODEL AND SUBJECT DETAILS

Non-human primate studies and samples

All animal studies and associated procedures were approved by the Monash University Animal Ethics Committee (identification no. 21659). Seven purpose-bred, experimentally naïve, adult male (7-16 years old) pigtail macaques (*Macaca nemestrina*) were utilized for the *in vivo* Vγ9Vδ2 T-cell expansion trial. All animals were housed in indoor-outdoor housing at the Monash Animal Research Platform Gippsland Field Station. The macaques were allocated into 1 of 4 treatment groups (1-2 animals per group; Table 1) for the trial. *In vivo* Vγ9Vδ2 T-cell expansion treatment protocols consisted of zoledronic acid monohydrate (Zol; 0.2mg/kg intravenous (IV) or 0.5mg intratracheal (IT); Sigma Aldrich), (E)-1-Hydroxy-2-methyl-2-butenyl 4-pyrophosphate (HMB-PP; 1mg/kg IV + 0.25mg IT; Sigma Aldrich), or Isopentenyl pyrophosphate (IPP; 0.5mg IT; Sigma Aldrich) once at day 0, along with subcutaneous (SC) recombinant human IL-2 (rhIL-2; $0.8x10^6$ IU SC q24h; Peprotech) for 5 days starting at day 0. IV antigen administrations were performed as 5-minute infusions (20mL total volume), and IT antigen administrations consisted of 5mL instillations at the approximate level of the thoracic inlet. Blood samples were collected at day 2, 4, 8, 15, and 22 post antigen treatment, and compared to paired baseline samples collected on day -14, -7, and 0. Bronchoalveolar lavage (BAL) fluid and rectal mucosal biopsies were collected at day 8 and 22 post antigen treatment and compared to paired samples taken pre-treatment (day -7). Inguinal lymph node biopsies were collected on day 8 and compared to paired samples taken pre-treatment (day -7).

In vitro Vγ9Vδ2 T-cell expansions were performed with cryopreserved samples from juvenile pigtail macaques involved in previous trials. All animals were acquired from the Australian National Macaque Breeding Colony. Details on the previous studies the macaques were enrolled in have been published separately.[29,97–100] All studies were approved by the relevant animal ethics committees.

Human ethics statement

Study protocols were approved by the University of Melbourne Human Research Ethics Committee (identification no. 11395), and all subjects provided written informed consent in accordance with the Declaration of Helsinki. All associated procedures were conducted in accordance with approved guidelines.

METHOD DETAILS

Sample collection and processing

Whole blood samples were collected into sodium heparin vacutainer tubes. Peripheral blood mononuclear cells (PBMCs) were isolated via Ficoll-Paque Plus density separation gradient (Human: 100% Ficoll; NHP: 95% Ficoll diluted with sterile PBS; Sigma Aldrich). Lymph node and rectal mucosal biopsy samples were mechanically dissociated, passed through 70μm cell strainers and resuspended in RPMI-1640 (Thermo Fisher Scientific) supplemented with 10% fetal calf serum (FCS) and 5% penicillin/streptomycin/glutamine (RF10).[101,102] Gastrointestinal tract samples were pre-digested in RF10 with Collagenase (0.1mg/mL; Sigma Aldrich) and DNase (1.5U/mL; Roche) for 2 hours at 37°C and 5% CO_2 with agitation, prior to mechanical dissociation. Macaque Vγ9Vδ2 T-cell phenotyping was performed on freshly isolated cells from PBMCs and tissues. The remaining samples were cryopreserved in 10% DMSO/ 90% FCS, and stored in liquid nitrogen. Human PBMCs were cryopreserved in 10%DMSO/ 90% FCS, prior to Vγ9Vδ2 T-cell phenotyping.

In vitro Vγ9Vδ2 T-cell expansion and stimulation

Cryopreserved pigtail macaque PBMCs or splenocytes were utilized for *in vitro* Vδ2 T-cell expansions. Bulk PBMC, seeded at $2e^6$ cells/mL, were cultured for 13 days in RF10 with Zol (15μM; Sigma Aldrich) and rhIL-2 ($1x10^3$ IU/mL, unless reported otherwise, Peprotech). For some experiments, $CCR6^+$ and $CCR6^-$ Vδ2 T-cells were isolated by cell sorting and expanded in autologous Vδ2 T-cell-depleted PBMCs ($1x10^6$ cells at $2x10^6$ cells/mL final concentration). Cell sorting consisted of viability dye and surface staining, and washing and resuspending the cells in PBS + 2% FCS. Samples were sorted with a BD FACS Aria III cell sorter. Vδ2 T-cell depletions were performed using anti-PE microbead (Miltenyi Biotec) following initial surface staining with unconjugated Vδ2 antibody (15D, Thermo Fisher Scientific) and a PE conjugated goat anti-mouse secondary antibody (polyclonal, Thermo Fisher Scientific). Microbead labelling and MACS depletions were performed according to the manufacturer's instructions. All expansions were incubated at 37°C and 5% CO_2. Media was replaced every 3-4 days (rhIL-2 was maintained throughout the culture period), and cultures were maintained at a maximum concentration of $2x10^6$ cells/mL.

For intracellular cytokine stimulations, cryopreserved PBMCs or tissue samples were stimulated with HMB-PP (20ng/mL, Sigma Aldrich) or paired unstimulated controls for 16hrs. *In vitro* expanded Vδ2 T-cells were mitogenically stimulated with Phorbol 12-Myristate 13-Acetate (0.025μg/mL, Abcam) and Ionomycin (0.04μg/mL, Sigma Aldrich) for 6 hours prior to antibody labelling, with paired unstimulated controls. GolgiStop and GolgiPlug (BD) were added after 1 hour to both stimulations and unstimulated controls. 72-hour cytokine stimulations were performed with rhIL-2 ($1x10^3$ IU/mL, Peprotech), or recombinant rhesus macaque IL-12 (rmIL-12; 50ng/mL; R and D Systems) and recombinant rhesus macaque IL-18 (rmIL-18; 50ng/mL; R and D Systems) in RF10. Where indicated, Zol (15μM; Sigma Aldrich), HMB-PP (20ng/mL, Sigma Aldrich), or IPP (4mg/mL; Sigma Aldrich) were included in the stimulations. All stimulations were performed at 37°C and 5% CO_2.

Single-cell TCR sequencing

$Vγ9^+Vδ2^+CD3^+CD20^-$Live/Dead$^-$ T-cells were dry-sorted into 96-well PCR Microplates (Axygen) with a BD FACSAria III cell sorter, and immediately sealed and stored at -20°C. cDNA synthesis was completed with a 25μl reaction volume consisting of: 5x First strand buffer (1x working concentration, 50mM Tris-HCl, 75mM KCl, 3mM $MgCl_2$, pH 8.3; Thermo Fisher Scientific), RNasin Plus® RNase inhibitor (8 units, Promega), dithiothreitol (DTT; 5mM; Thermo Fisher Scientific), igepal (0.25%; Sigma Aldrich), random hexamer primers (6ng/μl; Meridian Bioscience), dNTPs (0.8mM each; Bio Line), Superscript III (40 units, Thermo Fisher Scientific), and molecular grade water (Sigma Aldrich). Reverse transcription reactions were completed with the following thermal cycler profile: 42°C, 10min; 25°C, 10min; 50°C, 60min; 94°C, 5min. Amplification of the TRDV2/TRGV9 TCR chains was accomplished with a multiplex, nested PCR, similar to what has been previously described for αβTCR sequencing analysis.[103–107] Both initial and nested PCR reactions were completed with a 50μl reaction volume consisting of: 10x PCR buffer (1x working concentration, 15mM $MgCl_2$, pH 8.7; Qiagen), dNTPs (0.2mM each; Bio Line), the appropriate forward and reverse primers

(0.2μM each, Integrated DNA Technologies), HotStarTaq Plus DNA Polymerase (2.5 units; Qiagen), and molecular grade water (Sigma Aldrich). 5x Q solution (1x working concentration, Qiagen) was included in the nested PCR reactions. Initial and nested PCR reactions were completed with the following thermal cycler profile: 95°C, 5min (hot start); 94°C, 1min (denaturation); 56°C, 1min (annealing); 72°C, 1min (extension); and a final extension step (72°C, 10min) after 40 cycles were completed. PCR products were visualized on an agarose gel (1.5% agarose in 1x TAE, 1:10,000 SYBR Safe DNA gel stain; Thermo Fisher Scientific) to confirm the presence of an appropriately sized products, and samples were subsequently submitted for capillary electrophoresis sequencing (Macrogen, Inc).

PCR primer design

Previously published DNA oligonucleotide primers for macaque TRDV2, TRDC, TRGV9, and TRGC were utilized for the initial PCR reactions.[88] Nested DNA oligonucleotide primers were designed based on published macaque sequences within the initial PCR product (Table 2). The final PCR products contained a segment of the TRDV2/TRGV9 regions, the entire CDR3 region, and a segment of the TRDC/TRGC regions (TRDV2 amplicon length: 267bp; TRGV9 amplicon length: 282bp).

Antibodies and flow cytometry

To characterize macaque lymphocytes following *in vivo* or *in vitro* expansion, samples were washed 1x with PBS, and stained with LIVE/DEAD viability dye (Aqua, Blue, or Green; Thermo Fisher Scientific) to exclude dead cells. Samples were then incubated for 30-min at 4°C in the dark with various combinations of surface antibodies: Vδ2 FITC or unconjugated (15D, Thermo Fisher Scientific), Vγ9 FITC (7A5, Thermo Fisher Scientific), NKG2A APC (Z199, Beckman Coulter), CD94 APC (HP-3D9, BD), CXCR3 Alexa647 or Alexa700 or PE-Dazzle594 (G025H7, Biolegend), CD3 Alexa700 or BUV805 (SP34.2, BD), CD69 APC-Fire750 (FN50, Biolegend), CCR5 BV421 (J418F1, Biolegend), DNAM/CD226 BV605 (11A8, Biolegend), CD28 BV711 (CD28.2, BD), CCR6 BV785 (G034E3, Biolegend), CD20 BV510 or BUV805 or PE-CF594 (2H7, BD), EpCam/CD326 PE-CF594 (EBA-1, BD), CD26 Biotin (Clone5, in-house), CXCR5 PE-eFluor610 (MU5UBEE, Thermo Fisher Scientific), Vδ1 PE-Cy7 (TS8.2, Thermo Fisher Scientific), IL-18Rα PE-Vio770 (H44, Miltenyi Biotec), CD45 BUV395 or PE-Cy7 (D058-1283, BD), and CD95 BUV737 or PE-Cy7 (DX2, BD). When the unconjugated Vδ2 antibody was utilized to identify macaque Vγ9Vδ2 T-cells, the samples were pre-incubated with the unconjugated antibody for 30min, followed by a 30min incubation with a PE goat anti-mouse secondary antibody (polyclonal, Thermo Fisher Scientific), prior to surface staining. An in-house developed anti-CD26 antibody was utilized to identify macaque $CD26^{+}$ Vγ9Vδ2 T-cells (Jiang et al. Manuscript in preparation). CD26 antibody biotinylation was completed using a Type A Biotin Conjugation Kit (Abcam) per the manufacturer recommendations. Following surface staining with the biotinylated CD26 antibody, samples were incubated with a PE-TR Streptavidin secondary (Thermo Fisher Scientific). Samples were washed with PBS + 2% FCS following each surface incubation and fixed with BD Cytofix Fixation Buffer after surface staining. To evaluate transcription factor expression, cells were permeabilized with the BD Transcription buffer staining kit according to the manufacturer's recommendations, and subsequently labelled with transcription factor antibodies: Eomes PerCP-eFluor710 (WD1928, Thermo Fisher Scientific), Bcl6 Alexa647 (IG191E/A8, Biolegend), T-bet BV421 (4B10, Biolegend), and PLZF PE-CF594 (R17-809, BD). To evaluate cytokine or cytotoxic granule production, cells were permeabilized with BD Cytofix/cytoperm according to the manufacturer's recommendations, prior to intracellular antibody labelling: TNFα APC-Cy7 (Mab11, Biolegend), GM-CSF BV421 (BVD2-21C11, BD), Granzyme B BV510 (GB11, BD), IL-17A BV605 (BL168, Biolegend), and IFNγ BUV395 (B27, BD). All samples were analyzed on a BD LSRFortessa cell analyzer using BD FACSDiva.

QUANTIFICATION AND STATISTICAL ANALYSIS

Flow cytometry data from *in vitro* and *in vivo* experiments are presented as individual data points from individual animals +/- bars for the median and interquartile range (IQR). All associated statistical analysis and data presentation was performed using Prism (v9.4.1, GraphPad Software). Flow cytometry data was analyzed in FlowJo (v10.8.1, FlowJo LLC). Statistical analysis was completed with the indicated non-parametric tests in the figure legends. Fold change for cell expansions was calculated as a ratio of the final cell count divided by the initial cell count. *In vitro* Vγ9Vδ2 T-cell counts following expansion were calculated from total lymphocyte counts acquired with a CellDyn Emerald hematology analyzer (Abbott Laboratories), multiplied by the frequency of Vγ9Vδ2 T-cell as a percentage of the total lymphocyte population. TRDV2/TRGV9 sequences were processed using the MiXCR software package (v3.0.13; species: *Macaca mulatta*),[89] including sequence alignment and filtering to only include productive, paired TRDV2/TRGV9 CDR3 sequences for downstream analysis. All subsequent TCR

analysis and figure development was completed in R studio (v4.1.3; RStudio: Integrated Development Environment for R. RStudio, PBC) with the associated packages (Table S2) and code (https://github.com/BarberAxthelm/Vd2-Vg9_TCR_Analysis). Randomization tests were utilized to determine significance in diversity and richness differences between pre-expanded and *in vivo* expanded Vγ9Vδ2 T-cell populations in individual animals (n = 10,000 random distributions).[108] For all statistical tests, $p<0.05$ was considered statistically significant.